Evidence for a Paleogene boninitic arc following oceanic plateau-continent collision in the Western Cordillera of Colombia

Tomás Correa-Restrepo[a*], David M. Buchs[b,c], Cesar J. Vinasco-Vallejo[d], Sergio A. Restrepo-Moreno[d], Gabriel Rodríguez-García[a], Carlos A. Zuluaga-Castrillón[d]

[a]*Servicio Geológico Colombiano, Colombia*
[b]*Smithsonian Tropical Research Institute, Panama*
[c]*Cardiff University, United Kingdom*
[d]*Universidad Nacional de Colombia, Colombia*
**Corresponding author: tcorrea@sgc.gov.co*

Postprint version - figures are in the end.

ABSTRACT

The Caicedo Tuffs is a recently mapped Paleogene volcanic arc unit in the northern Andes, which provides insight into the magmatism of northwestern South America following its collision with the Caribbean-Colombian Oceanic Plateau (CCOP) in the latest Cretaceous. New regional geological mapping, igneous petrography, whole-rock and pyroxene geochemistry, and zircon U-Pb dating are provided for the northern sector of the eastern flank of the Western Cordillera of Colombia (Antioquia). These data reveal that the Caicedo Tuffs unit is predominantly composed of primary volcaniclastic deposits (tuff to breccia) that record mafic subaqueous volcanism and limited orogenic building shortly after collision of the CCOP. The geochemistry of these deposits includes major element characteristics and immobile trace element patterns that are typical of boninites. Zircons from these igneous rocks constrain a crystallization age of ca. 57 Ma, with meso-Proterozoic to Jurassic inherited zircons most likely reflecting continental recycling by turbidites in the subduction zone. The boninitic affinity of the Caicedo Tuffs and existing regional igneous and tectonic constraints can be explained by resuming of subduction and/or sinking of an older oceanic slab along northern South America following collision of the CCOP with South America. The boninitic, primary volcaniclastic deposits of the Caicedo Tuffs are crosscut by basaltic-gabbroic sills and dykes with oceanic plateau-like geochemical affinities, which lack evidence for hydrous melting and are compositionally similar to igneous rocks of the CCOP. These intrusions are interpreted to reflect decompression melting of plume-related mantle inherited during the collision of the CCOP with South America or slab detachment. The occurrence of oceanic plateau-like intrusions in a Paleocene volcanic arc casts doubt on the origin of other oceanic plateau sequences of the Western Cordillera, which are generally attributed to the Cretaceous CCOP. The Caicedo Tuffs is a unique boninite unit of which the detailed spatiotemporal extent and petrogenesis remain to be constrained, but that can provide valuable insight into tectono-magmatic processes during oceanic plateau-continent collision.

1. Introduction

The Western Cordillera of Colombia includes a complex lithostructural assemblage of Late Cretaceous to Paleogene oceanic sequences that formed by accretion of the Caribbean-Colombian Oceanic Plateau (CCOP), and associated intra-oceanic volcanic arcs, to northern South America in the latest Cretaceous, with subsequent emplacement of post-collisional volcanic arcs. Collisional convergence between the plateau and South America was oblique (Kennan and Pindell, 2009; Montes et al., 2019), leading to the preservation of

large scale (km-sized) lenticular stacks of oceanic sequences along the South American margin. These sequences offer unique insight into tectonic, sedimentary and magmatic processes associated with oceanic plateau-continent collision, but the exact number of accreted oceanic plateau(s), pre-collisional (intra-oceanic and continental) arcs, and post-collisional (continental) arcs remains uncertain. The timing of the collision and accretion of the oceanic sequences is mostly based on (a) the occurrence of continentally derived sediments in accreted or para-autochthonous sequences, with detrital zircons suggesting deposition shortly before and/or after collision (Botero et al., 2023; Montes et al., 2019; Pardo-Trujillo et al., 2020; Spikings et al., 2015; Vallejo et al., 2009; Villagómez et al., 2011; Zapata et al., 2020), (b) regional unconformities (Van Der Hammen, 1960; Villamil, 1999), and (c) thermochronological models (Villagómez and Spikings, 2013). In contrast, there is limited information for "orogenic" igneous rocks emplaced during and/or shortly after the CCOP-continent collision, associated with subduction dynamics.

We present here results of a new investigation stemming from 1:50,000 scale geological mapping of the eastern flank of the Western Cordillera of Colombia, that was carried out by the Colombian Geological Survey (Servicio Geologico Colombiano, SGC) between the municipalities of Caicedo and Anzá in the Antioquia Department (Correa-Restrepo et al., 2018, 2020) (Fig. 1). A new set of volcaniclastic rocks named Caicedo Tuffs ('Caicedo Vulcanites' in the SGC reports) was recognized as a post-collisional supra-subduction unit based on field, geochronological and geochemical features. The Caicedo Tuffs represent upper Paleocene (ca. 57 Ma) submarine volcanic arc sequences that offer a new insight into the Late Cretaceous to Paleogene geological evolution of western Colombia and the Northern Andes. Unusual (boninitic) geochemical characteristics of these rocks and their stratigraphic association with oceanic plateau-like igneous rocks notably suggest recycling of metasomatized and possibly plume-contaminated mantle shortly after collision of the CCOP with South America.

2. Geological background

The study area is located in the Northern Andes, more specifically in the septentrional portion of the Western Cordillera of Colombia, a region formed by allochthonous crustal blocks that include an assemblage of Late Cretaceous oceanic plateau, island arc(s) and sedimentary rocks that accreted against the continental margin in the latest Cretaceous, and were later locally cross-cut/covered by Paleogene volcanic arc sequences (Cediel et al., 2003; González, 2001; Pardo-Trujillo et al., 2020) (Fig. 1).

A large part of the Western Cordillera originated from the accretion of lavas and sill complexes of the Caribbean Colombian Oceanic Plateau (CCOP) and its cover of pelagic sedimentary rocks, which have collectively been included in the composite Dagua and Cañasgordas Groups (called together the Dagua-Cañasgordas Block in this contribution, Fig. 1) (e.g., Kerr et al., 1997; Nivia, 1996; Pardo-Trujillo et al., 2020; Pindell and Kennan, 2009). In the Western Cordillera and study area, oceanic plateau rocks have previously been ascribed to the San José de Urama Diabases unit (Correa-Restrepo et al., 2018, 2020; Rodríguez and Arango, 2013). Circum-Caribbean geochronological and biostratigraphic constraints suggest that the CCOP formed in the Pacific Ocean during several discrete phases of volcanism between ca. 145 and 85 (e.g., Andjić et al., 2019; Villagómez et al., 2011), before colliding and partly accreting with South America during the latest Cretaceous (e.g., Pindell et al., 2011; Vallejo et al., 2009). Although still poorly dated, consistent geochronological constraints exist in accreted plateau sequences of Colombia (Rodríguez and Arango, 2013; Villagómez et al., 2011).

The Cañasgordas Group in the northern part of the Western Cordillera includes volcanic arc sequences of the Barroso Formation, which consists of submarine volcanic sequences with subordinated, interbedded pelagic calcareous to siliceous and tuffaceous sedimentary rocks (Álvarez and González, 1978 and references therein). The volcanic rocks of the Barroso Formation and associate sedimentary rocks have been dated using

zircon U/Pb (LA-ICP-MS) and biostratigraphy markers yielding ages between the Barremian-Albian and the Campanian-Maastritchtian (Botero et al., 2023; Correa-Restrepo et al., 2018, 2020; Moreno-Sanchez and Pardo-Trujillo, 2003; Pardo-Trujillo et al., 2020 and references therein). There might be younger crystallization ages in this unit (57.2 ±1.3, U-Pb in zircon, Correa-Restrepo et al., 2018) that still need to be confirmed within an improved stratigraphic framework. In addition, younger Paleogene (ca. 58 Ma) U-Pb ages have also been reported in supra-subduction dykes cross-cutting Late Cretaceous metamorphic rocks of the Arquía Complex (an area chiefly between the Western and Central cordilleras of Colombia); these dykes might belong to another, post-collisional volcanic arc that remains to be documented more regionally (Zapata-Villada et al., 2021) within the Romeral Shear Zone.

The oceanic plateau and arc sequences of the San José de Urama Diabases and Barroso units are locally overlain by the Penderisco Formation, composed of pelagic, hemipelagic and siliciclastic (turbiditic systems) that deposited in the Late Cretaceous before/during collision of the CCOP and associated intra-oceanic volcanic arc(s) against South America (González and Londoño, 2003 and references therein). All these units are located to the west of the Cauca-Romeral Fault System, interpreted as the regional boundary between oceanic crustal rocks to the west (e.g., oceanic plateau and island arcs) and crustal units with predominant continental affinity to the east (Case et al., 1971; González, 1976; Vinasco, 2019).

Several Paleogene arc complexes crosscut and/or overlay the accreted Late Cretaceous units in western Colombia (Fig. 1). These complexes include the San Blas Complex, the Santa Cecilia La Equis Complex and the so-called Southwestern Complex (Barbosa-Espitia et al., 2019). The San Blas Complex is represented in Colombia by the Acandí Batholith and associated volcanic rocks (Cardona et al., 2018; Zapata-García and Rodríguez-García, 2020 and references therein), which have a cooling age of 48.1 ± 1 Ma (K/Ar age in sericite) and crystallization ages ranging between 48 and 42 Ma (U-Pb zircon) (Barbosa-Espitia et al., 2019 and references therein). The Santa Cecilia La Equis Complex is composed of the Santa Cecilia La Equis Formation and the Mandé Batholith (sometimes also referred to as “Dabeiba Arc”), with ages between 54 and 42 Ma (K/Ar in tonalite porphyry, Ar/Ar in basalts and plutonic rocks, U-Pb zircon in plutonic rocks and a tuff) (Barbosa-Espitia et al., 2019; Cardona et al., 2018; Zapata-García and Rodríguez-García, 2020 and references therein). All these units are considered part of the southeasternmost Panama intra-oceanic volcanic arc, which formed prior to collision of Panama with South America in the Cenozoic (Barbosa-Espitia et al., 2019; Cardona et al., 2018; León et al., 2018; Zapata-García and Rodríguez-García, 2020). From a tectonic perspective, these units belong to the Panamá-Chocó-Block (PCB) that is separated from the Western Cordillera (and study area) by the Dabeiba-Pueblo Rico Fault (Zapata-García and Rodríguez-García, 2020). The Western Cordillera of Colombia also includes the Timbiquí Complex with ages between 53 and 32 Ma (K/Ar, U-Pb zircon ages in andesites and dykes) (Barbosa-Espitia et al., 2019 and references therein). This unit belongs to the Southwestern Complex that was emplaced on top of the accreted CCOP after its collision with the continental margin of Colombia and Ecuador (Barbosa-Espitia et al., 2019; Kerr et al., 2002; Vallejo et al., 2009). All these units have tholeiitic to calc-alkaline geochemical affinities typical of supra-subduction magmatism of the PCB (Zapata-García and Rodríguez-García, 2020). Paleogene U-Pb in zircon ages of between 60 and 54 Ma have also been reported for continental-arc plutonic and subvolcanic rocks emplaced in the metamorphic complex of the Central Cordillera, with compositions that vary from diorites to tonalites, and include the Sonsón, Santa Bárbara and Antioquia Batholiths, as well as the El Bosque, El Hatillo, and Manizales stocks (Bayona et al., 2012; Bustamante et al., 2017) (Fig. 1).

3. Methods

3.1. Mapping and sampling

The 1:50,000-scale mapping projects carried out by the SGC (Correa-Restrepo et al., 2018, 2020) covered over 800 km2, of which about 72 km2 correspond to the new unit "Caicedo Tuffs". Cartographic transects were carried out along creeks, roads, ridges, and trails with control points every 500 m or less. Rock and saprolite samples were collected with the least weathered specimens exposed along streams. Polished thin sections were constructed for detailed petrography and major element mineral chemistry.

3.2. Whole rock and pyroxene geochemistry

Whole rock major oxides were analyzed at the geochemistry laboratory of the SGC in Bogotá, using an X-ray fluorescence spectrometer (ARL PERFORM'X) configured with OXSAS software for geological materials. Samples were grounded using tungsten carbide crusher and pulverizing mills (Retsch®). The weight of the samples for XRF analyzed was ca. 1 g. Trace elements were analyzed at ALS's laboratories. The samples were grounded to powder using a crusher (Terminator TM) and a pulverizing mill (Labtechnics LM2). About 0.1 g of pulverized sample was added to a lithium metaborate/lithium tetraborate flux, mixed and fused in a furnace at 1025 ◦C. The resulting melt was then cooled and dissolved in an acid mixture containing nitric, hydrochloric and hydrofluoric acids. This solution was then analyzed by inductively coupled plasma-mass spectrometry (ICP-MS). The quality control of the analyses carried out by ALS included 4 duplicates, 3 blanks and 5 standards (OREAS 24b, OREAS-45P, SY-4 and GRE-3).

Mineral chemistry microprobe analyses on pyroxene were performed on 5 polished thin sections, four of which belong to the Caicedo Tuffs and one of which is from the Barroso Formation. Pyroxenes were selected under a petrographic microscope, avoiding inclusions, fractures and alteration. Microprobe analyses were conducted on a JEOL JXA-8230 microprobe (Department of Geosciences, Universidad Nacional de Colombia) to quantify mineral chemistry and to further recognize reaction texture. Quantitative mineral compositions for major elements were collected using wavelength dispersive spectrometry (WDS) with an accelerating potential of 15 keV, beam currents of 20 nA and 50 nA, beam diameters varying from 1 µm to 10 µm, and acquisition times of 50 s. For major elements, accuracy and precision are of the order 1 to 2% relative according to careful sample preparation/selection and instrumental conditions. For elements with low concentrations (trace elements), detection limits are of the order of 100 ppm.

3.3. LA-ICP-MS U-Pb zircon dating

LA-ICP-MS U-Pb dating of zircons was conducted on 9 samples in the SGC at the U-Pb dating facility (Bogotá), following the procedure described in Peña et al. (2018). Analyses were performed on a Photon Machines laser ablation system with a 193 nm Excimer laser, coupled to an Element 2 mass spectrometer, using the isotopes ^{238}U, ^{206}Pb, and ^{204}Pb for manual integration, as well as the reference standards Plešovice, FC-1, Zircon 91,500, and Mount Dromedary. The points analyzed in the zircons were 20 µm in diameter. Data were reduced using the software Iolitev2.5® in IGORPro6.3.6.4®. Common lead correction was performed using the evolutionary model. Final results correspond to the mean data calculated after applying Chauvenet's criterion to eliminate spurious data more than two standard deviations from the mean. The U and Th concentrations were calculated using an external standard zircon. Ages were calculated and geochronological graphs were plotted using the software Isoplot V4.15. The isotopic results of the zircon ablations are shown in Supplementary Table 2 (ST2). SEM-BS images were obtained on the CARL ZEISS EVO MA10 electron microscope located at the Biomaterials Laboratory of the Universidad Nacional de Colombia, Medellín Campus.

4. Results

Data in the study area revealed the occurrence of oceanic plateau and arc-related sequences associated with the San Jose de Urama Diabases, Barroso, and Penderisco formations, similar to other sequences documented elsewhere in the Western Cordillera. However, most of the mapped area includes a new unit, introduced here as the "Caicedo Tuffs", which is the main focus of this study. 4.1. Field observations The Caicedo Tuffs were mapped as two irregular lenticular bodies of ca. 5 km2 and ca. 67 km2, northern and southern bodies, respectively, between the localities of Güintar and Tonusco Arriba (Fig. 1). The unit is bounded by volcanic and volcano-sedimentary rocks of the Barroso Formation (Cañasgordas Group). Pervasive weathering in the study area conceals major contacts, and so the boundaries between the Caicedo Tuffs and the Barroso Formation are inferred.

The Caicedo Tuffs generally exhibit a brecciated structure and are dark green. These volcanic breccias are monomictic, with a fragmental (altered) vitreous matrix and vitric to lithic clasts of basaltic to andesitic composition. The clasts are generally 2 mm to 15 cm in size and poorly sorted (Fig. 2a and b). They have sub-spherical, sub-angular to subrounded shapes. Amygdules filled with quartz, chlorite, prehnite and epidote are observed both in the vitreous matrix and in the lithics. Locally, the deposits are better sorted and appear stratified, laminated and/or graded. These sedimentary structures are more developed in sand-sized deposits (Fig. 2c). In many volcanic breccias the clasts show spheroidal weathering (Fig. 2d), while the matrix is completely altered to clayey products that generally retain the original fragmental structure. However, fresh pyroxene and plagioclase crystals are locally seen both in the altered vitric matrix and in the vitric to lithic clasts. Rare gabbroic sills (<3 m in thickness) locally intrude the tuffs (Fig. 2e).

4.2. Petrography and whole rock geochemistry

Twenty-three samples of igneous rocks from the Caicedo Tuffs area were selected for whole rock geochemical and petrographic analysis. Major and trace element results are presented in Table 1. Detailed petrographic information can be found in Supplementary Table 1 (ST1). Samples TCR-785 and FHO-404 (tuffs) were not considered in the interpretations because of their strong alteration associated with loss on ignition (LOI) values of 8.47 and 8.09 wt%, respectively. The rest of the samples exhibit slight to moderate alteration (LOI 1.75 to 6.54 wt%) that is consistent with microscope petrographic observations and geochemical results (see below).

Petrographic observations show that the volcanic breccias in the Caicedo Tuffs are predominantly composed of fragmented volcanic glass with minor mafic fine to coarse lithics, and only very rare possible massive lavas (e.g., sample TCR-1176 without clear stratigraphic control in the field). The volcanic glass is pervasively altered to clays and includes altered plagioclase, possible olivine and/or orthopyroxene replaced by serpentine, and locally fresh clinopyroxene. The basaltic clasts exhibit plagioclase and clinopyroxene crystals, often forming a fluidal texture. Pyroxenes are often uralitized and plagioclase is strongly sericitized. The coarser-grained igneous lithics are composed of plagioclase, clinopyroxene, quartz, pseudomorphs of mafic minerals (possibly olivine and/or orthopyroxenes), titanite and opaques. The plagioclase crystals are strongly altered to sericite and the clinopyroxene crystals are partially uralitized (Figs. 3a, b, d, e, and f). The dykes and sills correspond to quartz-gabbros/diorites with plagioclase, clinopyroxene and some quartz (Figs. 3h and i). The lavas comprise basalts with plagioclase, pyroxene, opaques and altered volcanic glass with subophitic and variolitic textures (Figs. 3c and g). Amygdules are observed both in the matrix and in the rock fragments of the tuffs. They are irregular to circular in shape, 0.01 mm to 2.5 cm in size, filled by quartz, prehnite, calcite, chlorite, and locally acicular epidote (Figs. 3a, b, d, e, and f).

Three main geochemical groups are considered in the study area (Table 1). Group 1 forms the bulk of the Caicedo Tuffs and corresponds to the matrix and clasts of the volcanic breccia as well as one lava sample

(sample TCR-1176). Group 2 corresponds to tuffaceous deposits lacking the typical dark green colour, weathering and erosion patterns seen elsewhere in the Caicedo Tuffs. Tectonic or stratigraphic relationships with the other geochemical groups was not observed. Group 3 corresponds to gabbroic and basaltic dykes and sills crosscutting the Caicedo Tuffs.

Geochemical results confirm that intense alteration has affected the studied igneous rocks, with LOI values ranging between 1.75 and 8.47 wt% (median = 3.5 wt%, n = 23, Table 1). Alteration is also indicated by discrepancies between classification diagrams based on mobile major elements (e.g., TAS) and immobile trace elements (e.g., Nb/Y vs. Zr/Ti diagram) (Figs. 4a and b, respectively). In these diagrams, Group 1 samples plot between the andesite and rhyodacite-dacite fields, whereas Group 2 and 3 samples plot in the basalt/andesite and andesite fields. Caution is however needed in the use of Zr/Ti ratio to estimate the degree of differentiation of Group 1 that has unusual Zr enrichment and whole rock compositions (see below). Because of significant alteration in the study area, a special emphasis is made here on the use of immobile trace elements to characterise the nature and origin of the igneous rocks.

Several of our samples classify as boninite according to the International Union of Geological Sciences (IUGS), with SiO_2 > 52 wt%, MgO > 8 wt% and TiO_2 < 0.5 wt% (Table 1). Because Si and Mg mobility is expected at the high level of alteration seen in the samples (e. g., Fig. 4a vs Fig. 4b), we used the boninite classification diagrams of Pearce and Reagan (2019) to further constrain the nature of these samples. This shows that most samples from Group 1 classify as High Silica Boninites (HSB) to high-Mg andesites that apparently define a continuous differentiation series. One sample from Group 2 plot in the lower end of the Low Silica Boninites (LSB) (Fig. 4c). However, when Mg and Si mobility diagrams are used (Pearce and Reagan, 2019), the sample from Group 2 does not meet the classification criteria for boninite (Fig. 4 d, e, f, g, and h). Samples from Group 3 do not plot in the boninite field in any of the diagrams. Although the general boninitic affinity of Group 1 is also supported by trace elements (see below), Si mobility is expected in our samples (see, e.g., the spread of SiO_2 values vs Cr, Fig. 4f). It is therefore not possible to confidently ascribe the samples to either low or high-Si boninite trends. Unfortunately, the high level of alteration of these boninites precludes detailed petrological investigation relying on fluid mobile elements (e.g., LILE).

In primitive mantle-normalized multielement diagrams (Fig. 5), Group 1 shows a progressive enrichment from HREE to LREE, with $(La/Lu)_N$ = 2.3–4.4. This group has positive Th, Zr and Hf anomalies, negative Nb and Ti anomalies, and $(Th/Nb)_N$ = 1.3–3.0. A distinctive characteristic of Group 1 that is typical of boninites is its low trace elements contents, with the least differentiated samples having HREE close to Primitive Mantle values. Group 2 shows a slight progressive enrichment from HREE to LREE with $(La/Lu)_N$ = 0.8–2.0, a variable negative Nb anomaly, and $(Th/Nb)_N$ = 0.6–0.9. Different from Groups 1 and 2, Group 3 shows an enrichment from LREE to HREE with $(La/Lu)_N$ = 0.6–0.9, a positive Nb anomaly, and $(Th/Nb)_N$ = 0.5–0.6. Groups 1 and 2 igneous rocks have trace element patterns typical of supra-subduction settings (i.e., negative Nb anomaly and enrichment in LREE and Th in PM-normalized multielement patterns), demonstrating volcanic arc origin(s). As further discussed below, Group 1 geochemistry is broadly similar to that of boninites from the northern termination of the Tongan Arc (Fig. 5). In contrast, Group 3 dykes and sills have an affinity more akin to oceanic plateau, as exemplified by the average reference values for the San Jose de Urama Diabases (SJUD) in Fig. 5. The detailed geochemical characteristics of these groups and their petrological significance are discussed in section 5.2 below.

4.3. Pyroxene geochemistry

Pyroxenes phenocrysts were analyzed by microprobe in 4 samples of crystal and lithic tuffs of the Caicedo Tuffs/Group 1 (TCR-1232A, TCR-1232B, TCR-1232C, TCR-1232E) and 1 sample of porphyritic basalt from the

nearby Barroso Formation (LM-199R). Representative pyroxene images with analyzed points are shown in Fig. 6 and chemical results are presented in Table 2.

Pyroxenes of the Caicedo Tuffs and the Barroso Formation have homogeneous augite compositions (Fig. 7a). However, pyroxenes in the Caicedo Tuffs are more magnesian (Mg# 77.7 to 91.2) than those in the sample of the Barroso Formation (Mg# 71.6 to 83.3). The pyroxenes of both units separate into two distinct groups, as shown in most geochemical diagrams (Fig. 7). Consistent with Mg# characteristics, clinopyroxenes of the Barroso Formation have higher TiO_2 and Al_2O_3 contents, whereas those of the Caicedo Tuffs exhibit a higher Cr_2O_3.

Decreasing TiO_2 and increasing Cr_2O_3 with decreasing Mg# is consistent with magmatic differentiation (Figs. 7b, and c). Despite geochemical differences, the clinopyroxenes of the two units plot in the tholeiitic volcanic arc field of Leterrier et al. (1982) tectonic discrimination diagrams (Figs. 7d, e and f). The analyzed crystals in both units exhibit mostly euhedral habit (Fig. 6), and their Mg# show disequilibrium with their carrier melt assuming $KD(Fe\text{-}Mg)_{cpx\text{-}liq}$ of 0.28 ± 0.08 (Putirka, 2008) (Fig. 8). Caution is however required in this observation considering the high degree of alteration of whole rocks in the Caicedo Tuffs unit (i.e., potentially affecting Mg#). Melt-clinopyroxene equilibrium tests using other components (e.g., Molendijk et al., 2022; Neave and Putirka, 2017) were not considered in the absence of Mg# equilibrium. Basaltic to basaltic andesitic compositions (Mg# = ~55–65) are suggested for the melt in equilibrium with the fresh clinopyroxenes (Fig. 8); this range is consistent with the differentiation trend of the Caicedo Tuffs based on whole rock compositions (Fig. 4). Although this suggests relative immobility of Mg and Fe in the altered whole rocks, we did not perform thermobarometric calculations because multicomponent Cpx-melt pairing and thermobarometric equations strongly rely on major elements that have been mobile in the studied altered rocks (e.g., Neave and Putirka, 2017; Putirka, 2008). Such elements include Na that was mobile in the altered boninites (Figs. 4a, b) but plays a key role in P-T estimates using Cpx-melt pairs. The Rhodes diagram may however indicate a dominantly antecrystic origin of the Cpx phenocrysts in the boninites (Fig. 8).

4.4. Geochronology

Approximately 30 samples of rock and saprolite from glassy, lithic and crystalline tuffs of the Caicedo Tuffs were considered for zircon extraction but only 9 yielded zircons, which were used for U-Pb-LA-ICP-MS analysis (Fig. 9). Cathodoluminescence images (SEM-CL) were obtained to determine the internal textures of zircons and select ablation points. The external morphology of zircons was assessed using SEM-BS images. Microscopically, most zircon crystals appear colourless to slightly yellow, translucent, with short to medium prismatic shapes and typical oscillatory zoning textures. Their size varies between 100 and 200 µm. Older crystals show homogeneous textures with no apparent zoning structure (Fig. 9a). In terms of crystal morphology, the pyramids tend to be more prominent than central prisms in the youngest (Paleogene) crystals. In contrast, the prisms tend to be much more prominent than pyramids in the older (Jurassic) crystals (Fig. 9b); the oldest (Proterozoic) crystals exhibit a rounded shape.

The Th/U ratio is higher than 0.1 for most of the data, with the exception of 10 results that include one with a Paleogene age (Fig. 10a). The concordant ages obtained are widespread from ca. 57 Ma (Paleogene) to ca. 2400 Ma (Paleoproterozoic). The Paleogene ages for four samples are considered crystallization ages for the Caicedo Tuffs (Fig. 10b and Fig. 11). These younger ages were found in 3 samples of Group 1 (TCR-1232A, TCR-1232B, and TCR-997) and sample FHO-404 that is very altered but also probably belong to the same geochemical group. Interestingly, 2 zircons show evidence of overgrowth according to CL images. These grains present rims with ages of 59.71 ± 1.35 Ma and 60.96 ± 1.35 Ma (Paleogene), with cores of 167.3 ± 3.7 Ma (Jurassic) and 256.92 ± 6.86 Ma (Permian), respectively (see red ellipse in Fig. 9a). These spatial relationships clearly demonstrate zircon magmatic overgrowth during the Paleogene at the expense of much older zircons.

This intragrain age variation is however rare in the studied samples where core and rim ages are commonly undistinguishable (e.g., sample FHO-404 in Fig. 9a).

5. Discussion

5.1. Evidence for Paleocene submarine arc volcanism in the Western Cordillera

Field observations, microscope petrography, and whole rock and mineral geochemical results indicate that the breccia forming most of the Caicedo Tuffs unit (i.e., geochemical Group 1 with boninitic affinities) is a primary volcaniclastic deposit formed by submarine volcanism. The relatively large size and glassy nature of most of the clasts in the unit is indicative of magma quenching in subaqueous conditions. In addition, the clasts are angular to subrounded, generally poorly sorted, and compositionally similar. They host a consistent population of clinopyroxenes with similar geochemical characteristics. These features are typical of primary volcaniclastic deposits that, by definition (White and Houghton, 2006), have not undergone extensive post-eruption reworking and mixing with compositionally distinct materials.

Although these deposits could be described as hyaloclastites, the latter are commonly associated with the emplacement, quenching, and brecciation of submarine (commonly pillowed) lavas (Cas and Wright, 1998; McPhie et al., 1993). Because pillow breccias do not occur in the Caicedo Tuffs, we suggest instead that the studied volcanic breccias are the result of fire fountains resulting from magma fragmentation in subaqueous conditions, indistinctively of deep or shallow marine settings (e.g., Cas and Simmons, 2018; Fujibayashi et al., 2014). These deposits are therefore best described as mafic tuffs. Layered and graded deposits found within the massive tuffs/primary volcanic breccias are likely the result of syn-volcanic turbidity currents forming on the slope of ocean volcanoes, or hemipelagic tephra fall deposits. No evidence exists for subaerial or coastal environments in the Caicedo Tuffs and, thus, it remains unclear if this unit has emplaced on the flanks of islands and/or seamounts. A Paleogene arc was previously reported in the Central Cordillera (Bayona et al., 2012 and references therein; Bustamante et al., 2017). The unique boninitic composition of the Caicedo Tuffs (see below) suggests it could represent an early magmatic phase of this volcanic arc. However, the Paleogene arc units in the Central Cordillera formed approximately 100 km to the southeast of the mapped area, thus suggesting that the Caicedo Tuffs unlikely formed in the same volcanic front.

Prior to this study, there was limited information on paleoenvironmental conditions that existed during the early Paleogene in the area that corresponds today to the northern Western Cordillera. Volcanic arc igneous rocks contemporaneous to the Caicedo Tuffs were recently documented by Zapata-Villada et al. (2021) in the Western Cordillera ~10 km from the study area. However, these nearby Paleogene arc rocks are only recorded by dykes crosscutting metamorphic rocks that formed during collision of the CCOP with South America (Arquía Complex), without clear indication of emplacement in subaqueous settings. Syn-collisional sedimentary rocks preserved in the Western Cordillera clearly indicate that subaqueous conditions existed on top of the CCOP shortly before/during its accretion with South America in the latest Cretaceous (Botero et al., 2023; Pardo-Trujillo et al., 2020). Submarine conditions seemed ubiquitous along northwestern South American margin at the time, despite that oceanic plateau had experienced a phase of subaerial volcanism before accretion (Buchs et al., 2018). Similarly, subaqueous environments in the Western Cordillera are documented by Eocene volcanic sequences that overlap accreted sequences of the CCOP (e.g., Barbosa-Espitia et al., 2019). In this context, the subaqueous facies of the Caicedo Tuffs provides an important control on the paleotopographic evolution of the continental margin shortly (ca. 5–10 Ma) after collision of the CCOP with South America. Regional observations of submarine sedimentation and volcanism suggest that the area did not develop a durable topography in the Paleogene. However, the arrival of oceanic plateaus in subduction zones is commonly associated with regional uplift, as notably illustrated by the accretion of an oceanic plateau in northern Costa Rica in the Cretaceous (Andjić et al., 2018), and by the collision of the

Ontong Java plateau with the Salomon arc in the Neogene (Mann and Taira, 2004). The apparent lack of uplift associated with oceanic plateau accretion in Colombia during the latest Cretaceous-early Paleogene could tentatively be related to oblique, as opposed to frontal, collision of the CCOP with South America (Kennan and Pindell, 2009; Montes et al., 2019; Pindell and Kennan, 2009). Limited orthogonal convergence with South America could have allowed detachment and accretion of oceanic plateau fragments along transcurrent fault systems, without extensive crustal shortening/uplift. Although the volcanic record of the study area (i.e., occurrence of subaqueous tuffs without evidence for coastal environments) supports limited post-collisional topography along the South American margin in the Paleocene, cooling of granitoids and metamorphic rocks east of the Western Cordillera during the latest Cretaceous to Paleocene (e.g., Villagómez and Spikings, 2013; Zapata-Villada et al., 2021) documents exhumation during collision of the CCOP with South America. Such exhumation could have been triggered by buoyancy contrasts in the upper asthenosphere and lithosphere and/or transcurrent forces associated with oblique collision of the CCOP, without need for significant orogenic building (see also the geodynamic discussion in section 5.3).

5.2. New constraints on the nature of supra-subduction magmatism following oceanic plateau-continent collision

Field crosscutting observations combined with new geochemical and geochronological results depict a complex supra-subduction igneous origin of the Caicedo Tuffs. Three geochemical groups can be recognized in the studied mafic to intermediate igneous rocks, with typical supra-subduction affinities of Groups 1 and 2 indicated by a negative Nb anomaly and enrichment of LREE and Th of whole rock compositions, as well as low-Ti clinopyroxenes (Figs. 5 and 7). Group 1 corresponding to primary volcanic breccias with a boninitic composition is consistently dated to ca. 57 Ma by 4 samples (Fig. 11). Additional age constraints are given by sheeted basaltic intrusions (dykes and sills) of Group 3 intruding the volcanic breccias of Group 1, indicating a contemporaneous or later emplacement for these rocks. Therefore, it is most likely that the Caicedo Tuffs relate to supra-subduction processes shortly (ca. 5–10 Ma) after, or possibly during, collision of the CCOP with South America (e.g., Villagómez and Spikings, 2013; Zapata-Villada et al., 2021). Limited exposures in the study area do not allow precise determining of the stratigraphic/tectonic relationship of Group 2 with respect to the Caicedo Tuffs (Group 1) and their cross-cutting dykes and sills (Group 3).

Comparison of the geochemical groups of the Caicedo Tuffs with typical igneous rocks of the Western Cordillera reveal important similarities and dissimilarities with Late Cretaceous to Eocene volcanic arc and oceanic plateau igneous suites in the region (Figs. 5 and 12). Critically, PM-normalized multiement, Nb/Yb vs Th/Yb (Pearce, 2008), La/ $Sm)_N$ vs (Th/Nb)N, and Dy/Yb vs Dy/Dy* (Davidson et al., 2013) diagrams show that Group 1 stands out as a unique supra-subduction igneous suite in the Western Cordillera. Consistent to its boninitic Mg, Si and Ti contents (Fig. 4), this group has very low levels of incompatible trace elements akin to those seen in intra-oceanic boninites of the Izu-Bonin and Tonga settings (e.g., Coulthard et al., 2021; Falloon et al., 2007, 2008; Shervais et al., 2021) (Fig. 5a). These levels are close to one order of magnitude lower than those seen in Setouchi boninites that are a rare occurrence of boninite in a continental setting (Pearce and Reagan, 2019; Tatsumi, 2006). This indicates that the Caicedo boninites, although found along South America, are distinct from the Setouchi continental boninites. Boninites of the Manihiki Plateau (Golowin et al., 2017; Pearce and Reagan, 2019) are another possible analogue to be considered here given that the Caicedo Tuffs are found in the Western Cordillera of Colombia that includes abundant oceanic plateau igneous rocks. However, Manihiki boninites that resulted from intra-oceanic plume magmatism (Golowin et al., 2017) lack the Nb negative anomaly typical of supra-subduction environments that is seen in Group 1. When compared to well documented occurrences of boninites in the Izu-Bonin and Tongan arcs, we find that the Caicedo Tuffs have trace element contents very similar to those of N Tonga boninites that formed by fluxed melting of depleted mantle with addition of Samoan plume components close to the northern termination of the Tongan

slab (Falloon et al., 2007, 2008). These boninites differ from those of the initiating Izu-Bonin Arc by a noticeable enrichment in HFSE and LREE, which was attributed to the addition of low volumes of a plume component (OIB-like melt) to otherwise depleted boninitic melts (e.g., Falloon et al., 2007). A similar HFSE and LREE enrichment is also seen in Group 1 (Fig. 5a). Caicedo and Tonga boninites are also similar in Nb/Yb vs Th/Yb and $La/Sm)_N$ vs $(Th/Nb)_N$ diagrams (Figs. 12a-b). However, the Caicedo boninites have a positive Zr-Hf anomaly in PM-normalized spectra, which is not seen in Tonga (Fig. 5a). This anomaly is typical of some boninites such as those of the Izu-Bonin Arc, where it was suggested that Zr/Sm (and Hf/Sm) fractionation may be due to (i) flux melting of gabbro veins in an otherwise refractory mantle (Pearce et al., 1999), or (ii) a shallow (amphibolite-facies) slab melt component (Li et al., 2019). In both cases, amphibole in the residue is believed to play an important control on the Zr/Sm ratio. This is however not evident from the Dy/Yb vs Dy/Dy* diagram (Davidson et al., 2013) that shows inconsistencies between the occurrence of the Zr-Hf anomaly and REEs characteristics in Caicedo, Izu-Bonin and Tonga boninites (Fig. 12c). In any case, immobile trace elements show that Group 1 is broadly similar, but not identical to, Tongan boninites that were interpreted to result from hydrous fluxing of a shallow refractory mantle source mixed with an OIB-like silicate melt during plume-subduction interaction (Falloon et al., 2008; Sobolev and Danyushevsky, 1994). As is further discussed below, the oceanic plateau-continent collision in South America could have provided the tectonic context required for similar petrological processes to form Group 1 boninites, without need for subduction initiation.

In contrast to boninites (and high-Mg andesites) of Group 1 that have a unique geochemical signature in Western Colombia, the composition of Group 2 closely resembles that of the Barroso Formation that represents a Late Cretaceous intra-oceanic volcanic arc that developed along the margin of the CCOP before its accretion to South America (Nivia and Gómez, 2005; Rodríguez and Arango, 2013; Villagómez, 2010; Weber et al., 2015; Zapata-Villada et al., 2017, 2021). This volcanic arc can be distinguished from post-collisional, Neogene supra-subduction magmatism in the Western Cordillera (e.g., Acandí, Santa Cecilia-La Equis, and Timbiquí volcanic arc units) based on its lower enrichment of LREE relative to HREE and lower $(Th/Nb)_N$ ratios (Figs. 5, 12a, and b) (Barbosa-Espitia et al., 2019; Cardona et al., 2018; Rodríguez and Arango, 2013). Because the occurrence of Group 2 is spatially very limited within the Caicedo Tuffs and regional occurrence of the Barroso Formation is widespread around this unit (Fig. 1), we consider that Group 2 represents thin tectonic (fault-bounded) slivers of the Barroso Formation within the Caicedo Tuffs.

Primary volcaniclastic breccia of the Caicedo Tuffs (boninitic Group 1) are crosscut by basaltic-gabbroic dykes and sills of Group 3 (Fig. 2e), which have oceanic plateau-like signatures (Figs. 5 and 12). The plateau-like affinity of this group is recognizable based on flat PM-normalized multielement patterns with a positive Nb anomaly (Figs. 5e-f), as well as location within the MORB-OIB array in the Nb/Yb vs Th/Yb diagram (Fig. 12a). The occurrence of oceanic plateau-like intrusions within the boninitic Caicedo Tuffs is a significant observation, because oceanic plateau rocks in the Western Cordillera are generally attributed to the Late Cretaceous CCOP (San José de Urama Diabases unit) (e.g., Rodríguez and Arango, 2013; Villagómez et al., 2011). However, Group 3 intrusions crosscut the volcanic deposits of Group 1, therefore unambiguously indicating a post-collisional, supra-subduction Paleogene (or younger) age. An oceanic plateau-like composition is not expected in a volcanic arc because supra-subduction magmatism is generally driven by dehydration and/or partial melting of the slab that leads to a distinct geochemistry with notably enrichment in Th and LREE and negative Nb-Ti anomalies (e.g., Kerr et al., 1997; Pearce, 2008). A simple petrological solution to the occurrence of CCOP-like (Group 3) dykes and sills within the Paleogene Caicedo Tuffs is that these rocks formed after accretion of the CCOP through adiabatic decompression and recycling of ancient mantle domains inherited from the margin of the CCOP during its collision with South America (see Fig. 13 and associated discussion below).

Additional constraints on post-collisional magmatism of the Caicedo Tuffs are provided by widespread zircon inheritance in Group 1 samples. The occurrence of inherited zircons in the Caicedo boninites can be explained in 3 mutually non-exclusive ways. First, zircons could have been supplied to the subduction zone from the Andean Block through subducting terrigenous sediments, as already suggested by several authors to explain the presence of zircon U-Pb age inheritances in volcanic arc rocks of the Western Cordillera (Barbosa-Espitia et al., 2019; Cetina et al., 2019; Correa-Restrepo et al., 2018). Second, zircons could have been assimilated by mafic melts during their ascent through units bearing older zircons, as for example the Cretaceous to Paleocene (?) Penderisco and Barroso formations (Botero, 2018; Correa-Restrepo et al., 2018; León et al., 2018). Permo-Triassic range interval are common in the Penderisco Formation and the more eastern domains (Central Cordillera) (Cochrane et al., 2014; Spikings et al., 2015; Vinasco et al., 2006), which could also explain the age distribution of zircons in the Caicedo Tuffs due to (minor) crustal assimilation. The presence of a significant population of Jurassic zircons in our results opens the possibility that there might be a still unknown Jurassic basement along the northwestern Andes, which was sampled by the studied Paleogene magmatism. Finally, zircon inheritance could relate to mantle metasomatism by felsic melts and metamorphic anatexis of basalts, which produce Zr-Hf and REE decoupling and are associated with crystallization of zircons in ultramafic to mafic rocks (Faithfull et al., 2018). Such metasomatic processes could have taken place in a refractory mantle before the formation of the boninites of the Caicedo Tuffs, possibly explaining the unusual Zr-Hf positive anomaly of Group 1 through scavenging of metasomatic/anatectic zircons from the refractory mantle. Given the ages of inherited zircons, this metasomatism is unlikely to have occurred in association with plume magmatism during the emplacement of the CCOP, but it could have occurred in an orogenic setting during the collision of the CCOP with South America. Testing between these different hypotheses would require isotopic data from the zircons and hosting volcanic rocks that are beyond the scope of this study. In any case, zircon inheritance indicates that the Caicedo boninites include a metasomatized mantle component, or minor crustal component(s) either associated with recycling of detrital zircons from subducting turbidites and/or magmatic assimilation of an arc to continental basement. These hypotheses are consistent with minor crustal components (sediment and/or altered oceanic crust) documented in other boninites (e.g., Falloon et al., 2008; Li et al., 2019; Pearce and Reagan, 2019).

In summary to the preceding discussion, mafic to intermediate igneous rocks of the Caicedo Tuffs depict a complex post-collisional magmatic context in the Western Cordillera during the Paleogene. A new, ca. 57 Ma-old supra-subduction, igneous suite with boninitic affinities is stratigraphically associated with ≤ 57 Ma-old oceanic plateau-like igneous rocks and tectonically juxtaposed to thin slivers of Late Cretaceous volcanic arc rocks (Barroso Formation). This unusual association of Paleogene rocks can be explained by (i) supra-subduction magmatism associated with flux melting of a refractory mantle source with metasomatic veins, (ii) recycling of ancient mantle domains originally associated with the emplacement (plume) of the CCOP, and (iii) possibly minor crustal assimilation by melts rising through the continental margin.

5.3. Relation to the tectonic evolution of the Western Cordillera

The Late Cretaceous oceanic plateau and volcanic arc assemblages of the Western Cordillera are commonly interpreted to have emplaced during oblique collision with South America, which led to crustal dismemberment during accretion and formation of large (km-sized), fault-bounded lenticular units along the continental margin (Pardo-Trujillo et al., 2020; Pindell and Kennan, 2009; Villagómez et al., 2011; Zapata-Villada et al., 2021). Tectonic and paleogeographic untangling is challenging in this context, and two main general models have been proposed to account for accreted sequences (Fig. 13), which we explain below to provide additional context for the formation of the Caicedo Tuffs.

The first model proposes the accretion of crustal slivers of the CCOP due to eastward-dipping subduction of oceanic lithosphere under the South American Plate (e.g., Burke et al., 1984; Kennan and Pindell, 2009; Nivia, 1996). A volcanic arc likely formed along a South American marginal basin that developed in the Late Cretaceous before the arrival and collision of the CCOP. Formation of this marginal basin and associated arc is supported by tholeiitic supra-subduction and back-arc igneous rocks of the Quebradagrande Complex in the Central Cordillera of Colombia (Cochrane et al., 2014; Nivia, 1996; Spikings et al., 2015; Villagómez et al., 2011). According to this model, oblique collision of the CCOP (a thickened oceanic crust) with South America produced an obstruction that caused subduction to jump westward, thus configuring a new oceanic arc above an east-dipping slab along the western margin of the CCOP. This volcanic arc is supported by the Barroso Formation and associated intrusives in the Western Cordillera ("Barroso Arc" in Fig. 13) (e.g., Correa-Restrepo et al., 2018, 2020; Rodríguez and Arango, 2013; Weber et al., 2015). The older slab subducting east of the CCOP detached during/after collision of the plateau with South America. However, a major limitation of this model is that the location of an arc along the southwestern margin of the CCOP at the time of formation of the Barroso Arc (105–81 Ma) is difficult to reconcile with available geological evidence and geometrical constraints from the early Caribbean area. The Panama volcanic arc initiated along the western margin of the CCOP ca. 72 Ma, as shown by biostratigraphic and geochronological data from in situ early arc sequences in Panama (e.g., Buchs et al., 2010; Wegner et al., 2011). Therefore, this arc cannot be correlative to the Barroso Arc of the Western Cordillera; some of the tectonic models ascribing a ca. 85 Ma subduction age in south Central America (e.g., Pindell and Kennan, 2009) are not supported by geological constraints from northern Costa Rica (Andjić et al., 2019 and references therein).

The second model (e.g., Jaramillo et al., 2017; Spikings et al., 2015; Vallejo et al., 2009; Villagómez et al., 2011; Zapata-Villada et al., 2021) proposes that the CCOP and South America were separated by an oceanic plate that subducted both (i) eastward under the South American Plate and possibly the Quebradagrande marginal basin in the east, and (ii) westward under the CCOP in the west, thus forming an intra-oceanic volcanic arc above the oceanic plateau. Similar to the first model above, the occurrence of the later volcanic arc is generally correlated to the Barroso Formation and contemporaneous granitoids in the Western Cordillera (e.g., Jaramillo et al., 2017; Montes et al., 2019; Villagómez et al., 2011). Therefore, this model favours a tectonic context similar to that of the Molucca Sea Plate today. The oceanic lithosphere separating the continent and oceanic plateau was fully subducted at the time of collision, leading to sinking of the oceanic lithosphere into the mantle, possibly without slab break-off (e.g., Jaramillo et al., 2017). Finally, similar to the first model, a subduction jump to the western side of the CCOP could have occurred during the collision, possibly leading to initiation of the Panama volcanic arc in the Late Cretaceous (e.g., Buchs et al., 2010). A major limitation of this model is that it remains unclear when the plateau collided with South America between Ecuador and Colombia (e.g., Kennan and Pindell, 2009; Montes et al., 2019), and when and to what extent the plateau subducted beneath South America in the Paleogene (e.g., Bayona et al., 2012). Therefore, to account for this uncertainty, we provide two plausible scenarios for the post-collisional setting of this model (Fig. 13b).

New data on Paleocene magmatism from northwestern South America can offer valuable constraints on subduction dynamics associated with collision of the CCOP. Zapata-Villada et al. (2021) recently showed that Paleocene (ca. 58 Ma) basaltic dykes crosscutting metamorphic rocks of the Arquía Complex have a possible adakatic signature. Although not very pronounced, this adakitic signature suggests post-collisional partial melting of mafic crust. In the context of existing tectonic reconstructions, such melting could be explained either by post-collisional slab detachment (Fig. 13a), slab sinking (Fig. 13b), or partial melting of a flat slab during subduction of the CCOP (Fig. 13b). The occurrence of boninites crosscut by oceanic plateau-like intrusions in the Caicedo Tuffs offers important constraints on the nature of magmatic process following collision of the CCOP with South America. The petrogenesis of boninites is commonly accounted for by flux melting of a refractory (typically harzburgitic) mantle by hydrous siliceous slab melts at shallow depth (Pearce

and Reagan, 2019, and references therein). Although commonly associated with subduction initiation, such petrogenesis is not restricted to nascent arc systems (Pearce and Reagan, 2019) and has notably been found at the northern termination of the Tonga Arc close to the Samoan plume (e.g., Falloon et al., 2007). The age of formation of the Caicedo boninites and the tectonic complexity of Colombia cannot be accommodated by a single Late Cretaceous subduction initiation in the circum-Caribbean region (Whattam and Stern, 2015). As explained above, the tectonic evolution of northern South America between the latest Cretaceous to Paleocene requires several subduction jumps associated with oceanic plateau-continent collision and arc accretion(s). This offers the possibility for Paleocene subduction initiation along the (non-continental) crust of the CCOP accreted along South America (Fig. 13). Boninites (and high-Mg andesites) of the Caicedo Tuffs (Group 1) could have resulted from shallow melting of a depleted (sub-CCOP?) mantle during subduction initiation (Fig. 13, models a and b2). Alternatively, post- to syn-collisional slab detachment/sinking in the Paleocene could have provided required conditions to generate boninites with or without subduction initiation (Fig. 13, models a and b1). Although the Tonga and Caicedo boninites are compositionally similar and suggest involvement of a plume component in the Caicedo boninites, the timing of formation of the Caicedo Tuffs (Paleocene) and regional age constraints from accreted CCOP sequences (Late Cretaceous) do not support involvement of an active plume in the petrogenesis of Caicedo boninites. However, Cretaceous plume magmatism associated with formation of the CCOP could have metasomatized the sub-CCOP mantle, leading to trace element enrichments similar to those observed during plume-subduction interaction in Tonga, and possibly explaining the occurrence of Zr-Hf anomalies in the Caicedo boninites. Another possible component that could have contributed to the formation of Tonga-like boninites in Colombia is partial melting of CCOP crust during shallow slab subduction (Fig. 13, model b2). In the aforementioned tectonic contexts, formation of plateau-like Group 3 cross-cutting Group 1 boninites could be explained by adiabatic melting of sub-CCOP mantle that rose due to asthenospheric flow formed by slab detachment (Fig. 13a) or slab sinking (Fig. 13b). The range of hypotheses presented here outlines that, similar to uncertainties undermining our understanding of the Late Cretaceous to Paleocene tectonic evolution of Colombia, much uncertainties remain regarding possible tectono-magmatic processes associated with the formation of the Caicedo Tuffs.

6. Conclusions

The Caicedo Tuffs record the occurrence of a new Paleogene (ca. 57 Ma) volcanic front in the Western Cordillera, which postdates latest Cretaceous to earliest Cenozoic collision of the CCOP (San José de Urama Diabases) and associated intra-oceanic volcanic arc (Barroso Formation) with South America. The primary volcaniclastic facies of the Caicedo Tuffs supports submarine volcanism. In addition, no evidence for subaerial environments was found in the study area. This suggests that the outermost margin of northwestern South America had a relatively smooth topography in the Paleocene despite recent, and possibly still on-going, collision of the CCOP with South America. The subdued topography and the lenticular assemblage of plateau- and arc-related crustal fragments in the Western Cordillera (Fig. 1) suggest that oblique collision of the oceanic plateau with the continent (Kennan and Pindell, 2009; Montes et al., 2019; Pindell and Kennan, 2009) could have controlled the accretion of oceanic sequences and the exhumation of metamorphic rocks (Villagómez and Spikings, 2013; Zapata-Villada et al., 2021), without causing significant orogenesis/mountain building.

The Caicedo Tuffs are mostly composed of boninitic igneous rocks with immobile trace element contents similar to those of Tonga boninites. Caicedo boninites are however partly distinct with notably a positive Zr-Hf anomaly in normalized multi-element patterns. The compositional characteristics of the Caicedo boninites suggest flux melting of a refractory mantle source at shallow depth following collision of the CCOP with South America. This could be explained by resuming of subduction and/or detachment/sinking of oceanic slabs from older volcanic arcs that accreted along South America during the collision (Fig. 13). The geochemical similarity

of Caicedo and Tonga boninites (especially their higher HFSE and LREE compared to Izu-Bonin boninites) suggest that a plume component could also have contributed to the formation of Caicedo boninites. This could be related to, e.g., (i) pre-collisional mantle metasomatism by the Caribbean plume in the sub-CCOP lithosphere, and/or (ii) syn- to post-collisional melting of CCOP crust in an orogenic context. Despite inheritance of meso-Proterozoic to Jurassic zircons in the Caicedo Tuffs, there is no geochemical evidence for significant crustal components at the source of the boninites, as is also observed in other boninites (Falloon et al., 2007, 2008; Li et al., 2019). The most likely (but not unique) source for inherited zircons in the Colombian boninites is derivation from South America by terrigenous sediments (e.g., turbidites) recycled in a subduction zone.

The Caicedo boninites are crosscut by basaltic and gabbroic dykes with plateau-like geochemical affinities. Plateau-like intrusions in the supra-subduction Caicedo Tuffs could reflect anhydrous, decompression melting of ancient plume-related mantle inherited from the collision of the CCOP with South America (Fig. 13). The occurrence of plateau-like intrusions in a Paleocene supra-subduction unit is an important observation for our understanding of regional geology. Many studies have suggested that oceanic plateau igneous rocks of the Western Cordillera are Late Cretaceous and associated with the formation of the CCOP in an intra-oceanic environment. In contrast, our results show that some of these oceanic plateau-like igneous rocks may represent a previously-unidentified, younger magmatic phase that remains to be confirmed and identified regionally.

There is still much uncertainty on the regional extent of the Caicedo Tuffs as well as the exact tectonic setting and petrological processes associated with the formation of the boninites and oceanic plateau-like rocks of this unit. However, contemporaneous emplacement of the Caicedo Tuffs (this study) and adakitic dykes in the nearby Arquía Complex (Zapata-Villada et al., 2021) suggests the occurrence of a compositionally unusual Paleocene volcanic arc in northwestern South America, which was likely associated with a new volcanic front after/ during collision of the CCOP with South America, and formed as a response to subduction initiation and/or detaching/sinking slab(s) ("Caicedo Arc" in Fig. 13). Further study of this arc could offer valuable insight into tectono-magmatic processes associated with oceanic plateau-continent collision and the formation of boninites.

Declaration of Competing Interest

The authors declare that they have no known competing financial interests or personal relationships that could have appeared to influence the work reported in this paper.

Acknowledgements

We are grateful to Scott Whattam and an anonymous reviewer for their constructive comments that helped significantly improve this manuscript. We thank the Servicio Geológico Colombiano (SGC) for funding and supporting the project; Universidad Nacional de Colombia for the mineral geochemistry, the SEM-BS images and the Faculty Scholarship for the first author; Grant #GEFNE137-15 of the National Geographic Society for the analysis of whole rock trace elements; the Petrography and Chemistry Laboratories of the SGC for preparing the thin sections and for the major elements analysis; Francy H. Ortiz, Juan P. Zapata, Milton G. Obando, Lina M. Cetina, ángela M. Rincón, Juan R. Peláez, Faustino Mosquera, Manuel Castro and Professor John Jairo Sánchez for their contributions in the field and discussions; Jimmy A. Muñoz of the Geochronology Laboratory of the SGC for performing the U-Pb zircon radiometric dating.

Appendix A. Supplementary data

Supplementary data to this article can be found online at https://doi.org/10.1016/j.lithos.2023.107313

References

Alvarez, E., González, H., 1978. Geología y geoquimica del cuadrangulo I-7, URRAO. Instituto Nacional de Investigaciones Geológico Mineras.

Andjic, G., Baumgartner, P.O., Baumgartner-Mora, C., 2018. Rapid vertical motions and formation of volcanic arc gaps: Plateau collision recorded in the forearc geological evolution (Costa Rica margin). Basin Res. 30 (5), 863–894. https://doi.org/10.1111/bre.12284.

Andjic, G., Baumgartner, P.O., Baumgartner-Mora, C., 2019. Collision of the Caribbean large Igneous Province with the Americas: Earliest evidence from the forearc of Costa Rica. GSA Bull. 131 (9–10), 1555–1580. https://doi.org/10.1130/B35037.1.

Barbosa-Espitia, A.A., Kamenov, G.D., Foster, D.A., Restrepo-Moreno, S.A., Pardo- Trujillo, A., 2019. Contemporaneous Paleogene arc-magmatism within continental and accreted oceanic arc complexes in the northwestern Andes and Panama. Lithos 348–349 (september), 105185. https://doi.org/10.1016/j.lithos.2019.105185.

Bayona, G., Cardona, A., Jaramillo, C., Mora, A., Montes, C., Valencia, V., Ayala, C., Montenegro, O., Ibañez-Mejia, M., 2012. Early Paleogene magmatism in the northern Andes: Insights on the effects of Oceanic Plateau-continent convergence. Earth Planet. Sci. Lett. 331–332, 97–111. https://doi.org/10.1016/j.epsl.2012.03.015.

Botero, M., 2018. Proveniencia y estilo estructural de la Formaciión Penderisco y las Sedimentitas de Beibaviejo en el corte Uramita-Dabeiba: relación con la evolución del Bloque Panamá– Chocá (PCB). M.Sc Thesis. Universidad Nacional de Colombia.

Botero, M., Vinasco, C.J., Restrepo Moreno, S.A., Foster, D., Kamenov, G.D., 2023. Caribbean–South America interactions since the late cretaceous: insights from Zircon U-Pb and Lu-Hf Isotopic data in sedimentary sequences of the Northwestern Andes. SSRN Electron. J. 123 (October 2022), 104231 https://doi.org/10.2139/ssrn.4264590.

Buchs, D.M., Arculus, R.J., Baumgartner, P.O., Baumgartner-Mora, C., Ulianov, A., 2010. Late cretaceous arc development on the SW margin of the Caribbean Plate: Insights from the Golfito, Costa Rica, and Azuero, Panama, complexes. Geochem. Geophys. Geosyst. 11 (7), https://doi.org/10.1029/2009GC002901.

Buchs, D.M., Kerr, A.C., Brims, J.C., Zapata-Villada, J.P., Correa-Restrepo, T., Rodríguez, G., 2018. Evidence for subaerial development of the Caribbean oceanic plateau in the late cretaceous and palaeo-environmental implications. Earth Planet. Sci. Lett. 499 https://doi.org/10.1016/j.epsl.2018.07.020.

Burke, K., Cooper, C., Dewey, J.F., Mann, P., Pindell, J.L., 1984. Caribbean tectonics and relative plate motions. Mem. Geol. Soc. America 162 (1), 31–63. https://doi.org/ 10.1130/MEM162-p31.

Bustamante, C., Cardona, A., Archanjo, C.J., Bayona, G., Lara, M., Valencia, V., 2017. Geochemistry and isotopic signatures of Paleogene plutonic and detrital rocks of the Northern Andes of Colombia: a record of post-collisional arc magmatism. Lithos 277, 199–209. https://doi.org/10.1016/j.lithos.2016.11.025.

Cardona, A., León, S., Jaramillo, J.S., Montes, C., Valencia, V., Vanegas, J., Bustamante, C., Echeverri, S., 2018. The Paleogene arcs of the northern Andes of Colombia and Panama: Insights on plate kinematic implications from new and existing geochemical, geochronological and isotopic data. Tectonophysics 749 (October), 88–103. https://doi.org/10.1016/j.tecto.2018.10.032.

Cas, R.A.F., Simmons, J.M., 2018. Why Deep-Water Eruptions are so different from Subaerial Eruptions. Front. Earth Sci. 6 https://doi.org/10.3389/feart.2018.00198.

Cas, R.A.F., Wright, J.V., 1998. Volcanic successions: Modern and Ancient, A geological approach to processes products and successions. In: Chapman and Hall, UK, 39. https://doi.org/10.1007/978-0-412-44640-5.

Case, J.E., Duran, S., Alfonso, L.G., L. R, Moore, W.R., 1971. Tectonic investigations in western Colombia and eastern Panama. Bull. Geol. Soc. Am. 82 (10), 2685–2712. https://doi.org/10.1130/0016-7606(1971)82[2685:TIIWCA]2.0.CO;2.

Cediel, F., Shaw, R.P., Cáceres, C., 2003. Tectonic Assembly of the Northern Andean Block. In: Bartolini, C., Buffler, R.T., Blickwede, J.F. (Eds.), The Circum-Gulf of Mexico and the Caribbean: Hydrocarbon Habitats, Basin Formation, and Plate Tectonics, 79, pp. 815–848.

Cetina, L.M., Tassinari, C.C., Rodríguez, G., Correa-Restrepo, T., 2019. Origin of premesozoic xenocrystic zircons in cretaceous sub-volcanic rocks of the northern Andes (Colombia): paleogeographic implications for the region. J. S. Am. Earth Sci. 96 https://doi.org/10.1016/j.jsames.2019.102363.

Cochrane, R., Spikings, R., Gerdes, A., Ulianov, A., Mora, A., Villagómez, D., Putlitz, B., Chiaradia, M., 2014. Permo-Triassic anatexis, continental rifting and the disassembly of western Pangaea. Lithos 190–191, 383–402. https://doi.org/10.1016/j.lithos.2013.12.020.

Correa-Restrepo, T., Obando, M.G., Zapata, J.P., Rincón, A.V., Ortiz, F.H., Rodríguez, G., Cetina, L.M., 2018. Geología del borde Occidental de la Plancha 130 Santa Fe de Antioquia. Escala 1:50.000. Memoria Explicativa. Servicio Geológico Colombiano, p. 545. http://recordcenter.sgc.gov.co/B22/542_18GeologiaBordeOccl_130/Documento/Pdf/InfoFinalBordeOccidentalPl30.pdf.

Correa-Restrepo, T., Obando-Quintero, M.G., Ortiz-Párraga, F.H., Tobón-Mazo, M.J., Peláez-Gaviria, J.R., Zapata-Villada, J.P., Rodríguez-García, G., 2020. Geología del Borde Occidental de la Plancha 146 Medellín Occidental. In: Cartografía a escala 1: 50.000. Memoria Explicativa. Servicio Geológico Colombiano. http://recordcenter.sgc.gov.co/B23/735%7B%5C_%7D2020GeolBordeOccPl146/Documento/Pdf/MemExplGeolBordeOccPl146.pdf.

Coulthard, D.A., Reagan, M.K., Shimizu, K., Bindeman, I.N., Brounce, M., Almeev, R.R., Ryan, J., Chapman, T., Shervais, J., Pearce, J.A., 2021. Magma Source Evolution following Subduction Initiation: evidence from the Element Concentrations, Stable Isotope Ratios, and Water Contents of Volcanic Glasses from the Bonin Forearc (IODP Expedition 352). Geochem. Geophys. Geosyst. 22 (1) https://doi.org/10.1029/2020GC009054.

Davidson, J., Turner, S., Plank, T., 2013. Dy/Dy*: Variations arising from mantle sources and petrogenetic processes. J. Petrol. 54 (3), 525–537. https://doi.org/10.1093/petrology/egs076.

Faithfull, J.W., Dempster, T.J., MacDonald, J.M., Reilly, M., 2018. Metasomatism and the crystallization of zircon megacrysts in Archaean peridotites from the Lewisian complex, NW Scotland. Contrib. Mineral. Petrol. 173 (12), 99. https://doi.org/10.1007/s00410-018-1527-5.

Falloon, T.J., Danyushevsky, L.V., Crawford, T.J., Maas, R., Woodhead, J.D., Eggins, S. M., Bloomer, S.H., Wright, D.J., Zlobin, S.K., Stacey, A.R., 2007. Multiple mantle plume components involved in the petrogenesis of subduction-related lavas from the northern termination of the Tonga Arc and northern Lau Basin: evidence from the geochemistry of arc and backarc submarine volcanics. Geochem. Geophys. Geosyst. 8 (9) https://doi.org/10.1029/2007GC001619.

Falloon, T.J., Danyushevsky, L.V., Crawford, A.J., Meffre, S., Woodhead, J.D., Bloomer, S.H., 2008. Boninites and adakites from the northern termination of the Tonga Trench: Implications for adakite petrogenesis. J. Petrol. 49 (4), 697–715. https://doi.org/10.1093/petrology/egm080.

Fujibayashi, N., Asakura, K., Hattori, T., Allen, S., 2014. Pillow lava and spasmodic submarine fire fountaining in the middle Miocene marginal basin, Sado Island, Japan. Island Arc 23 (4), 344–364. https://doi.org/10.1111/iar.12091.

Golowin, R., Portnyagin, M., Hoernle, K., Hauff, F., Gurenko, A., Garbe-Sch¨onberg, D., Werner, R., Turner, S., 2017. Boninite-like intraplate magmas from Manihiki Plateau require ultra-depleted and enriched source components. Nat. Commun. 8 https:// doi.org/10.1038/ncomms14322.

Gómez Tapias, J., Montes, N.E., Nivia, A., Diederix, H., 2015. Mapa Geológico de Colombia 2015. Escala 1:1'000.000. Servicio Geológico Colombiano, p. 2. González, H., 1976. Geologia del Cuadrangulo J-8, Sonson - Memoria Explicativa. Instituto Nacional de Investigaciones Geológico Mineras (INGEOMINAS). http://catalogo.sgc.gov.co/cgi-bin/koha/opac-detail.pl?biblionumber=11610.

González, H., 2001. Mapa Geológico del Departamento de Antioquia. Geología, Recursos Minerales y Amenazas Potenciales. Escala 1:400.000 - Memoria Explicativa. In: Ingeominas. González, H., Londoño, A.C., 2003. Geología de las Planchas 129 Cañasgordas y 145 Urrao. Memoria Explicativa, escala 1:100.000. Ingeominas.

Jaramillo, J.S., Cardona, A., León, S., Valencia, V., Vinasco, C., 2017. Geochemistry and geochronology from cretaceous magmatic and sedimentary rocks at 6◦35′ N, western flank of the Central cordillera (Colombian Andes): Magmatic record of arc growth and collision. J. S. Am. Earth Sci. 76, 460–481. https://doi.org/10.1016/j.jsames.2017.04.012.

Kennan, L., Pindell, J.L., 2009. Dextral shear, terrane accretion and basin formation in the Northern Andes: best explained by interaction with a Pacific-derived Caribbean plate? Geol. Soc. Spec. Publ. 328 (December), 487–531. https://doi.org/10.1144/SP328.20.

Kerr, A., Marriner, G., Tarney, J., Nivia, A., Saunders, A., Thirlwall, M., Sinton, C., 1997. Cretaceous Basaltic Teeranes in Western Colombia: Elemental, Chonological and Sr- Nd Isotopic Constraints on Petrogenesis. J. Petrol. 38 (6), 677–702.

Kerr, A.C., Aspden, J.A., Tarney, J., Pilatasig, L.F., 2002. The nature and provenance of accreted oceanic terranes in western Ecuador: Geochemical and tectonic constraints. J. Geol. Soc. 159 (5), 577–594. https://doi.org/10.1144/0016-764901-151.

Leal-Mejía, H., 2011. Phanerozoic Gold Metallogeny in the Colombian Andes: A Tectono- Magmatic Approach. Doctoral Thesis. Universitat de Barcelona.

León, S., Cardona, A., Parra, M., Sobel, E.R., Jaramillo, J.S., Glodny, J., Valencia, V.A., Chew, D., Montes, C., Posada, G., Monsalve, G., Pardo-Trujillo, A., 2018. Transition from Collisional to Subduction-Related Regimes: an example from Neogene Panama- Nazca-South America Interactions. Tectonics 37 (1), 119–139. https://doi.org/10.1002/2017TC004785.

Leterrier, J., Maury, R.C., Thonon, P., Girard, D., Marchal, M., 1982. Clinopyroxene composition as a method of identification of the magmatic affinities of paleovolcanic series. Earth Planet. Sci. Lett. 59 (1), 139–154. https://doi.org/10.1016/0012-821X(82)90122-4.

Li, H.Y., Taylor, R.N., Prytulak, J., Kirchenbaur, M., Shervais, J.W., Ryan, J.G., Godard, M., Reagan, M.K., Pearce, J.A., 2019. Radiogenic isotopes document the start of subduction in the Western Pacific. Earth Planet. Sci. Lett. 518, 197–210. https://doi.org/10.1016/j.epsl.2019.04.041.

Mann, P., Taira, A., 2004. Global tectonic significance of the Solomon Islands and Ontong Java Plateau convergent zone. Tectonophysics 389 (3–4), 137–190. https://doi.org/10.1016/j.tecto.2003.10.024.

McDonough, W.F., Sun, S., s., 1995. The composition of the Earth. Chem. Geol. 120 (3–4), 223–253. https://doi.org/10.1016/0009-2541(94)00140-4.

McPhie, J. Jocelyn, Doyle, M. Mark, Allen, R. Rodney, University of Tasmania. Centre for Ore Deposit and Exploration Studies, 1993. Volcanic Textures : A Guide to the Interpretation of Textures in Volcanic Rocks, p. 198.

Molendijk, S.M., Buchs, D.M., Mason, P.R.D., Blundy, J.D., 2022. Clinopyroxene diversity and magma plumbing system processes in an accreted Pacific Ocean island, Panama. Contrib. Mineral. Petrol. 177 (2), 30. https://doi.org/10.1007/s00410-022-01894-w.

Montes, C., Rodriguez-Corcho, A.F., Bayona, G., Hoyos, N., Zapata, S., Cardona, A., 2019. Continental margin response to multiple arc-continent collisions: the northern Andes-Caribbean margin. Earth Sci. Rev. 198, 102903 https://doi.org/10.1016/j.earscirev.2019.102903.

Moreno-Sanchez, M., Pardo-Trujillo, A., 2003. Stratigraphical and Sedimentological Constraints on Western Colombia: Implications on the Evolution ofthe Caribbean Plate. In: AAPG Memoir, 79, Issue December, pp. 891–924.

Morimoto, N., Fabries, J., Ferguson, A.K., Ginzburg, I.V., Ross, M., Seifert, F.A., Zussman, J., Aoki, K., Gottardi, G., 1988. Nomenclature of Pyroxenes Subcommittee on Pyroxenes Commission on New Minerals and Mineral Names International Mineralogical Association, 73(for Ml). American Mineralogist, pp. 1123–1133.

Neave, D.A., Putirka, K.D., 2017. A new clinopyroxene-liquid barometer, and implications for magma storage pressures under Icelandic rift zones. Am. Mineral. 102 (4), 777–794. https://doi.org/10.2138/am-2017-5968.

Nivia, A., 1996. Complejo Estructural Dagua, Registro de Deformación de la Provincia Litosférica Oceánica Cretácica Occidental, un Prisma Acrecionario. In: VII Congreso Colombiano de Geología, pp. 54–67.

Nivia, A., Gómez, J., 2005. El Gabro de Santa Fe de Antioquia y la Cuarzodiorita de Sabanalarga, una propuesta de nomenclatura litoestratigráfica para dos cuerpos plutónicos diferentes agrupados previamente como Batolito de Sabanalarga en el departamento de Antioquia, Colombia. X Congreso Colombiano de Geol. 1–11 https://doi.org/10.13140/RG.2.1.4322.0240.

Pardo-Trujillo, A., Cardona, A., Giraldo, A.S., León, S., Vallejo, D.F., Trejos-Tamayo, R., Plata, A., Ceballos, J., Echeverri, S., Barbosa-Espitia, A., Slattery, J., Salazar-Ríos, A., Botello, G.E., Celis, S.A., Osorio-Granada, E., Giraldo-Villegas, C.A., 2020. Sedimentary record of the Cretaceous–Paleocene arc–continent collision in the northwestern Colombian Andes: Insights from stratigraphic and provenance constraints. Sediment. Geol. 401, 105627 https://doi.org/10.1016/j.sedgeo.2020.105627.

Pearce, J.A., 2008. Geochemical fingerprinting of oceanic basalts with applications to ophiolite classification and the search for Archean oceanic crust. LITHOS 100, 14–48. https://doi.org/10.1016/j.lithos.2007.06.016.

Pearce, J.A., Reagan, M.K., 2019. Identification, classification, and interpretation of boninites from Anthropocene to Eoarchean using Si-Mg-Ti systematics. Geosphere 15 (4), 1008–1037. https://doi.org/10.1130/GES01661.1.

Pearce, J.A., Kempton, P.D., Nowell, G.M., Noble, S.R., 1999. Hf-Nd element and isotope perspective on the nature and provenance of mantle and subduction components in Western Pacific Arc-basin systems. J. Petrol. 40 (11), 1579–1611. https://doi.org/ 10.1093/petroj/40.11.1579.

Peña, M.L., Muñoz, J., Urueña, C., 2018. Avances sobre datación U-Pb en circones mediante la técnica LA-ICP-MS Servicio Geológico Colombiano. Boletí. Geológ. 44, 39–56.

Pindell, J.L., Kennan, L., 2009. Tectonic evolution of the Gulf of Mexico, Caribbean and northern South America in the mantle reference frame: an update. Geol. Soc. Spec. Publ. 328 (June), 1–55. https://doi.org/10.1144/SP328.1.

Pindell, J., Maresch, W.V., Martens, U., Stanek, K., 2011. The Greater Antillean Arc: early cretaceous origin and proposed relationship to central American subduction mélanges: implications for models of Caribbean evolution. Int. Geol. Rev. 54 (2), 131–143. https://doi.org/10.1080/00206814.2010.510008.

Putirka, K.D., 2008. Thermometers and barometers for volcanic systems. Rev. Mineral. Geochem. 69, 61–120. https://doi.org/10.2138/rmg.2008.69.3.

Rodríguez, G., Arango, M.I., 2013. Formación Barroso : Arco Volcánico Toleitico Y Diabasas De San José De Urama : Un Prisma Acrecionario T-Morb En El Segmento Norte De La Cordillera Occidental De Colombia. Boletín Ciencias de La Tierra 33, 17–38. ISSN0120-3630. Rubatto, D., 2002. Zircon trace element geochemistry : distribution coefficients and the link between U-Pb ages and metamorphism Zircon trace element geochemistry : partitioning with garnet and the link between U – Pb ages and metamorphism. Chem. Geol. 184 (February), 123–138. https://doi.org/10.1016/S0009-2541(01)00355-2.

Shervais, J.W., Reagan, M.K., Godard, M., Prytulak, J., Ryan, J.G., Pearce, J.A., Almeev, R.R., Li, H., Haugen, E., Chapman, T., Kurz, W., Nelson, W.R., Heaton, D.E., Kirchenbaur, M., Shimizu, K., Sakuyama, T., Vetter, S.K., Li, Y., Whattam, S., 2021. Magmatic Response to Subduction Initiation, Part II: Boninites and Related Rocks of the Izu-Bonin Arc from IOPD Expedition 352. Geochem. Geophys. Geosyst. 22 (1), 1–34. https://doi.org/10.1029/2020GC009093.

Sobolev, A.V., Danyushevsky, L.V., 1994. Petrology and geochemistry of boninites from the north termination of the Tonga trench: Constraints on the generation conditions of primary high-Ca boninite magmas. J. Petrol. 35 (5), 1183–1211. https://doi.org/10.1093/petrology/35.5.1183.

Spikings, R., Cochrane, R., Villagomez, D., Van der Lelij, R., Vallejo, C., Winkler, W., Beate, B., 2015. The geological history of northwestern South America: from Pangaea to the early collision of the Caribbean large Igneous Province (290-75 Ma). Gondwana Res. 27 (1), 95–139. https://doi.org/10.1016/j.gr.2014.06.004.

Tatsumi, Y., 2006. High-Mg andesites in the Setouchi volcanic belt, Southwestern Japan: Analogy to Archean magmatism and continental crust formation? Annu. Rev. Earth Planet. Sci. 34, 467–499. https://doi.org/10.1146/annurev.earth.34.031405.125014.

Vallejo, C., Winkler, W., Spikings, R.A., Luzieux, L., Heller, F., Bussy, F., 2009. Mode and timing of terrane accretion in the forearc of the Andes in Ecuador. Mem. Geol. Soc. America 204 (June), 197–216. https://doi.org/10.1130/2009.1204(09).

Van Der Hammen, T., 1960. Estratigrafía del terciario y maestrichtiano continentales y tectogénesis de los Andes colombianos. Boletín de Geología, VI, pp. 67–128.

Villagómez, D., 2010. Thermochronology, geochronology and geochemistry of the Western and Central cordilleras and Sierra Nevada de Santa Marta, Colombia: The tectonic evolution of NW South America. Faculté Des Sciences, p. 144. PhD(0000). http://archive-ouverte.unige.ch/unige:14270.

Villagómez, D., Spikings, R., 2013. Thermochronology and tectonics of the Central and Western Cordilleras of Colombia: early Cretaceous-Tertiary evolution of the Northern Andes. Lithos 160–161 (1), 228–249. https://doi.org/10.1016/j.lithos.2012.12.008.

Villagómez, D., Spikings, R., Magna, T., Kammer, A., Winkler, W., Beltrán, A., 2011. Geochronology, geochemistry and tectonic evolution of the Western and Central cordilleras of Colombia. Lithos 219–221. Villamil, T., 1999. Campanian-Miocene tectonostratigraphy, depocenter evolution and basin development of Colombia and western Venezuela. Palaeogeogr. Palaeoclimatol. Palaeoecol. 153 (1–4), 239–275. https://doi.org/10.1016/S0031-0182(99)00075-9.

Vinasco, C., 2019. The romeral shear zone. In: Frontiers in Earth Sciences, pp. 833–876. https://doi.org/10.1007/978-3-319-76132-9_12.

Vinasco, C.J., Cordani, U.G., González, H., Weber, M., Pelaez, C., 2006. Geochronological, isotopic, and geochemical data from Permo-Triassic granitic gneisses and granitoids of the Colombian Central Andes. J. S. Am. Earth Sci. 21 (4), 355–371. https://doi.org/10.1016/j.jsames.2006.07.007.

Weber, M., Gómez-Tapias, J., Cardona, A., Duarte, E., Pardo-Trujillo, A., Valencia, V.A., 2015. Geochemistry of the Santa Fé Batholith and Buriticá Tonalite in NW Colombia - evidence of subduction initiation beneath the Colombian Caribbean Plateau. J. S. Am. Earth Sci. 62 (December 2017), 257–274. https://doi.org/10.1016/j.jsames.2015.04.002.

Wegner, W., Worner, G., Harmon, R.S., Jicha, B.R., 2011. Magmatic history and evolution of the central American Land Bridge in Panama since cretaceous times. Geol. Soc. Am. Bull. 123 (3–4), 703–724. https://doi.org/10.1130/B30109.1.

Whattam, S., Stern, R., 2015. Late cretaceous plume-induced subduction initiation along the southern margin of the Caribbean and NW South América: the first documented example with implications for the onset of plate tectonics. Gondwana Res. 27, 38–63.

White, J.D.L., Houghton, B.F., 2006. Primary volcaniclastic rocks. Geology 34 (8), 677. https://doi.org/10.1130/G22346.1.

Zapata, S., Patiño, A., Cardona, A., Parra, M., Valencia, V., Reiners, P., Oboh- Ikuenobe, F., Genezini, F., 2020. Bedrock and detrital zircon thermochronology to unravel exhumation histories of accreted tectonic blocks: an example from the Western Colombian Andes. J. S. Am. Earth Sci. 103 (April) https://doi.org/10.1016/j.jsames.2020.102715.

Zapata-García, G., Rodríguez-García, G., 2020. New Contributions to Knowledge about the Chocó-Panamá Arc in Colombia, Including a New Segment South of Colombia. Geología de Colombia 3, 417–450. Zapata-Villada, J.P., 2018.

Registro magmático y metamórfico en una zona de colisión Cretácica en la margen occidental de la Cordillera Central: Implicaciones tectónicas en los Andes del Norte. M.Sc Thesis. Universidad Nacional de Colombia sede Medellín.

Zapata-Villada, J.P., Restrepo, J.J., Cardona-Molina, A., Martens, U., 2017. Geoquímica y geocronología de las rocas volcánicas básicas y el Gabro de Altamira, Cordillera Occidental (Colombia): Registro de ambientes de plateau y arco oceánico superpuestos durante el cretácico. Bolet. Geol. 39 (2), 13–30. https://doi.org/10.18273/revbol.v39n2-2017001.

Zapata-Villada, J.P., Cardona, A., Serna, S., Rodríguez, G., 2021. Late cretaceous to Paleocene magmatic record of the transition between collision and subduction in the Western and Central Cordillera of northern Colombia. J. S. Am. Earth Sci. 112 (April), 103557 https://doi.org/10.1016/j.jsames.2021.103557.

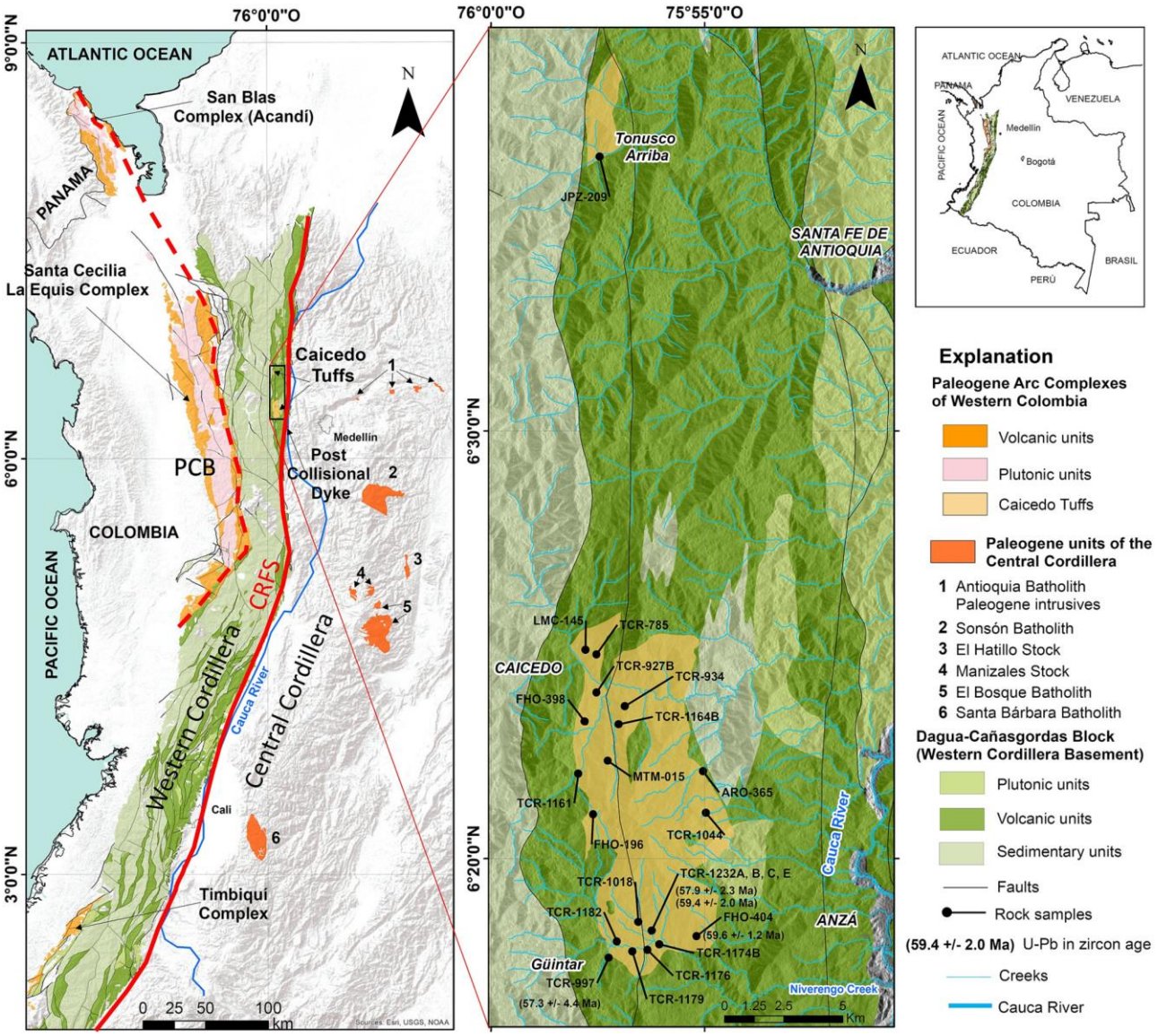

Figure 1. Location of the Caicedo Tuffs in western Colombia. The geologic units (other than the Caicedo Tuffs) and faults are from the Geologic Map of Colombia (Gómez Tapias et al., 2015). Location of the Paleogene units of the Central Cordillera after Leal-Mejía (2011). Location of the Post Collisional Dyke (PCD) was taken from Zapata-Villada et al. (2021). Polygons of the Caicedo Tuffs were modified from Correa-Restrepo et al. (2020, 2018). CRFS: Cauca-Romeral Fault System (approximate fault system trace marked with continuous red line); PCB: Panama-Chocó Block (approximate eastern boundary marked with a red dashed line).

Figure 2. Macroscopic aspect of the Caicedo Tuffs. **a.** General brecciated structure of the unit (upper basin of the Niverengo Creek, nearby Güintar village); **b.** Autoclasts in vitric breccia (middle basin of the Niverengo Creek, boundaries marked with white dashed lines in the picture); **c.** Layered ash-sized vitric tuff/volcaniclastic turbidites (middle basin of the Niverengo Creek); **d.** Aspect of the alteration with remnants of original clasts and spheroidal weathering (nearby Tonusco Arriba); **e.** Plateau-like gabbroic sill (Sample TCR-1174B) intruding the Caicedo Tuffs (Middle basin of the Niverengo Creek; boundaries marked with white dashed lines in the picture).

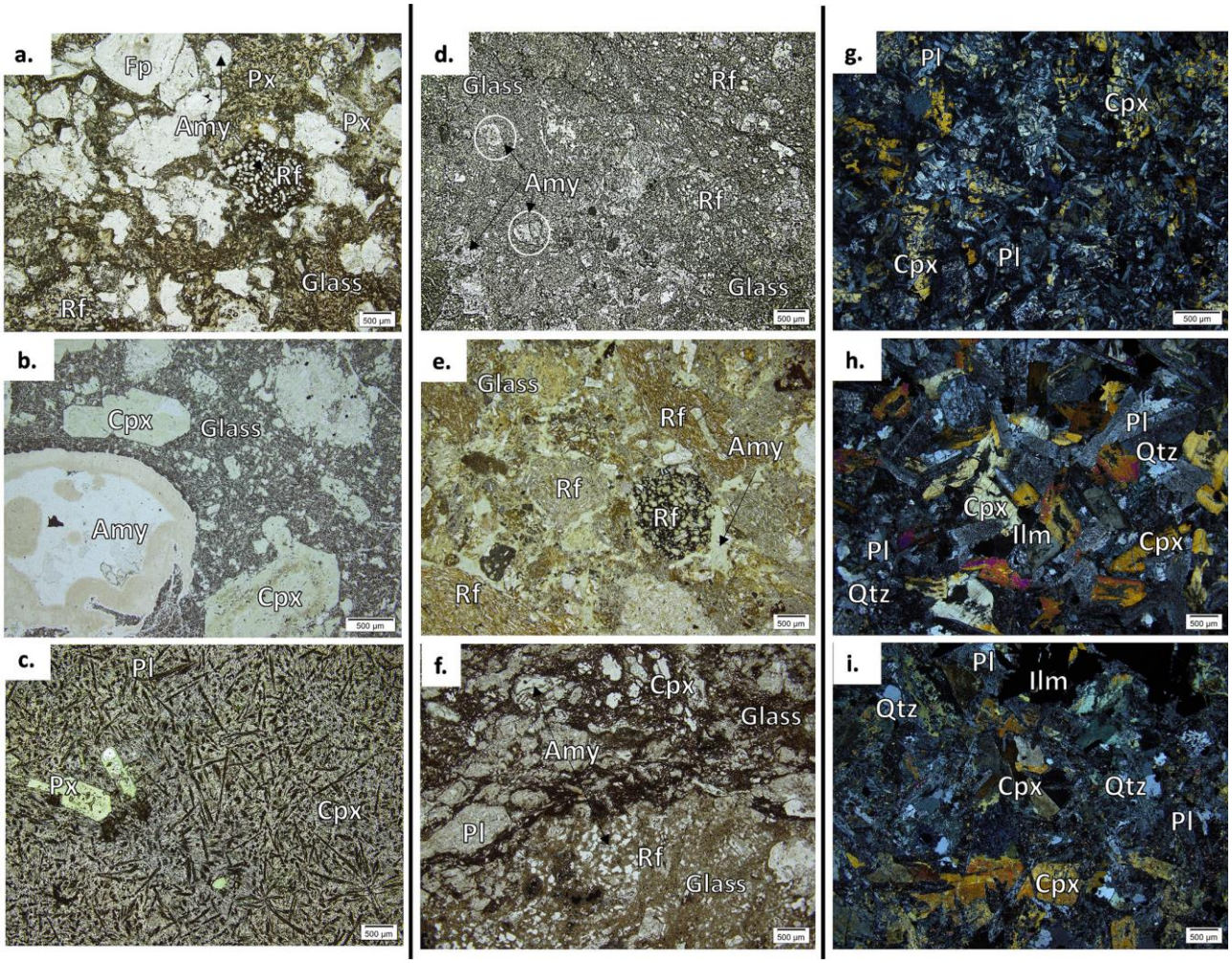

Figure 3. Representative thin sections of the Caicedo Tuffs. **a.** TCR-1232A (tuff); b. FHO-398 (basaltic clast); **c.** TCR-1176 (basaltic lava); d. ARO-365 (tuff); **d.** JPZ-209 (tuff); **e.** (tuff); **f.** TCR-1044 (tuff); g. MTM-015 (basalt); **h.** TCR-1174B (quartz-gabbro); **i.** TCR-1164B (quartz-gabbro). Qtz: Quartz, Pl: Plagioclase, Rf: Rock Fragment, Fp: Ferromagnesian pseudomorph, Cpx: Clinopyroxene, Amy: Amygdule, Glass: Volcanic Glass, Ilm: Ilmenite.

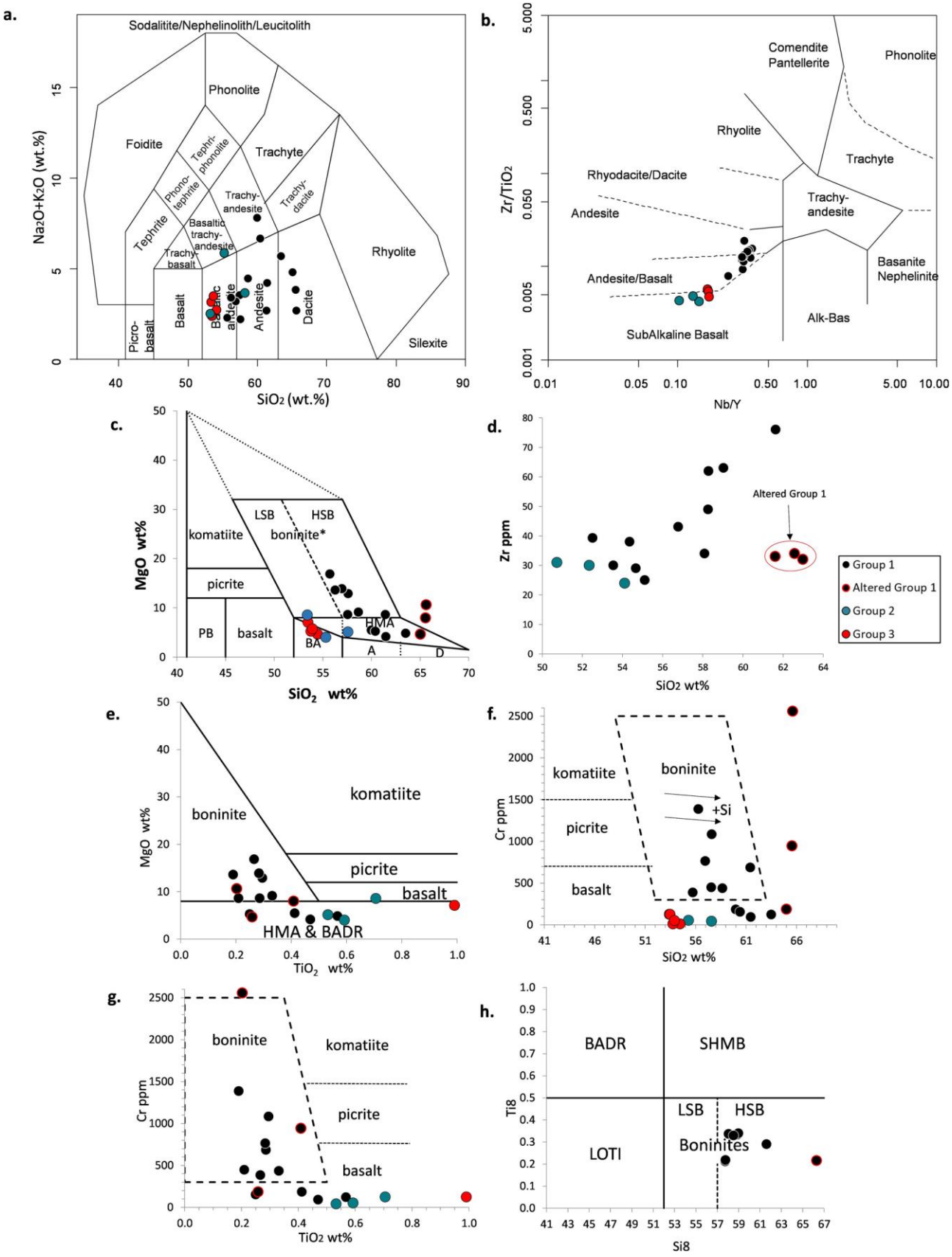

Figure 4. Whole rock geochemical classification diagrams for the Geochemical Groups. **a.** SiO_2 vs. $Na_2O + K_2O$ (wt%); **b.** Nb/Y vs. Zr/Ti diagram; **c.** SiO_2 vs. MgO (wt%); **d.** TiO2 vs. MgO (wt%); **e.** SiO2 vs. MgO (wt%); **f.** TiO2 (wt%) vs. Cr (ppm); **g.** Si_8 vs. Ti_8 (wt%); **e.** SiO2 (wt%) vs. Zr (ppm). Diagrams c, d, e, f, g and h after Pearce and Reagan (2019).

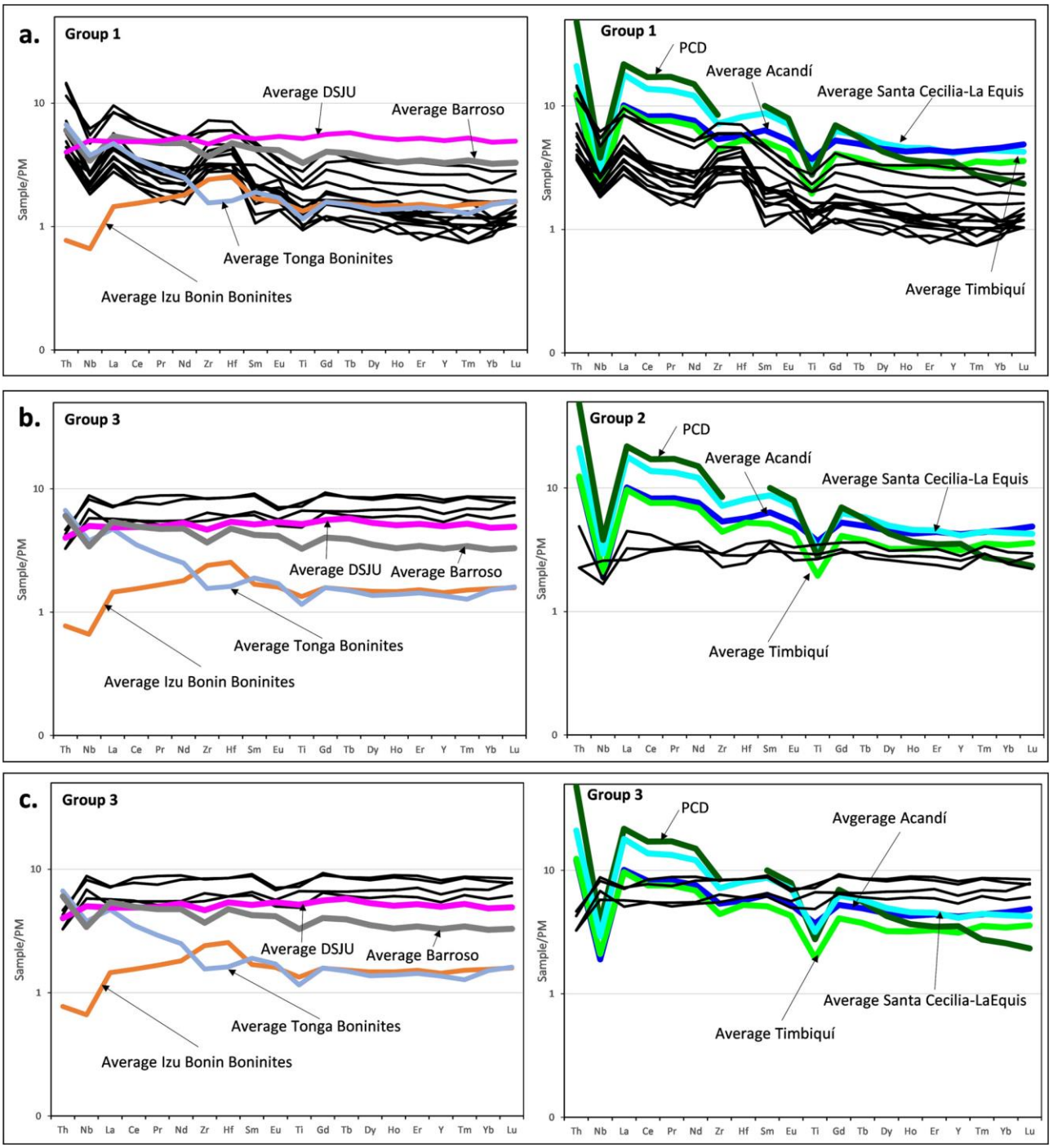

Figure 5. Geochemistry of Groups 1, 2, 3 and reference values normalized to the Primitive Mantle (PM) of McDonough et al. (1995). A. Comparison of Geochemical Group 1 with the reference values; b. Comparison of Geochemical Group 2 with the reference values; c. Comparison of Geochemical Group 3 with the reference values. The Barroso Formation and San Jose de Urama Diabases (SJUD) are pre-collision intra-oceanic volcanic arc and oceanic plateau units with values from Rodríguez and Arango (2013). The Acandí, Timbiquí and Santa Cecilia La Equis represent post-collision volcanic arcs with values from Barbosa-Espitia et al. (2019). A post-collisional dyke (PCD) from the Western Cordillera is taken from Zapata-Villada (2018) (see text for further explanations). Values for the Izu-Bonin Boninites from Shervais et al. (2021). Values for the Tonga Boninites from (Falloon et al., 2007, 2008).

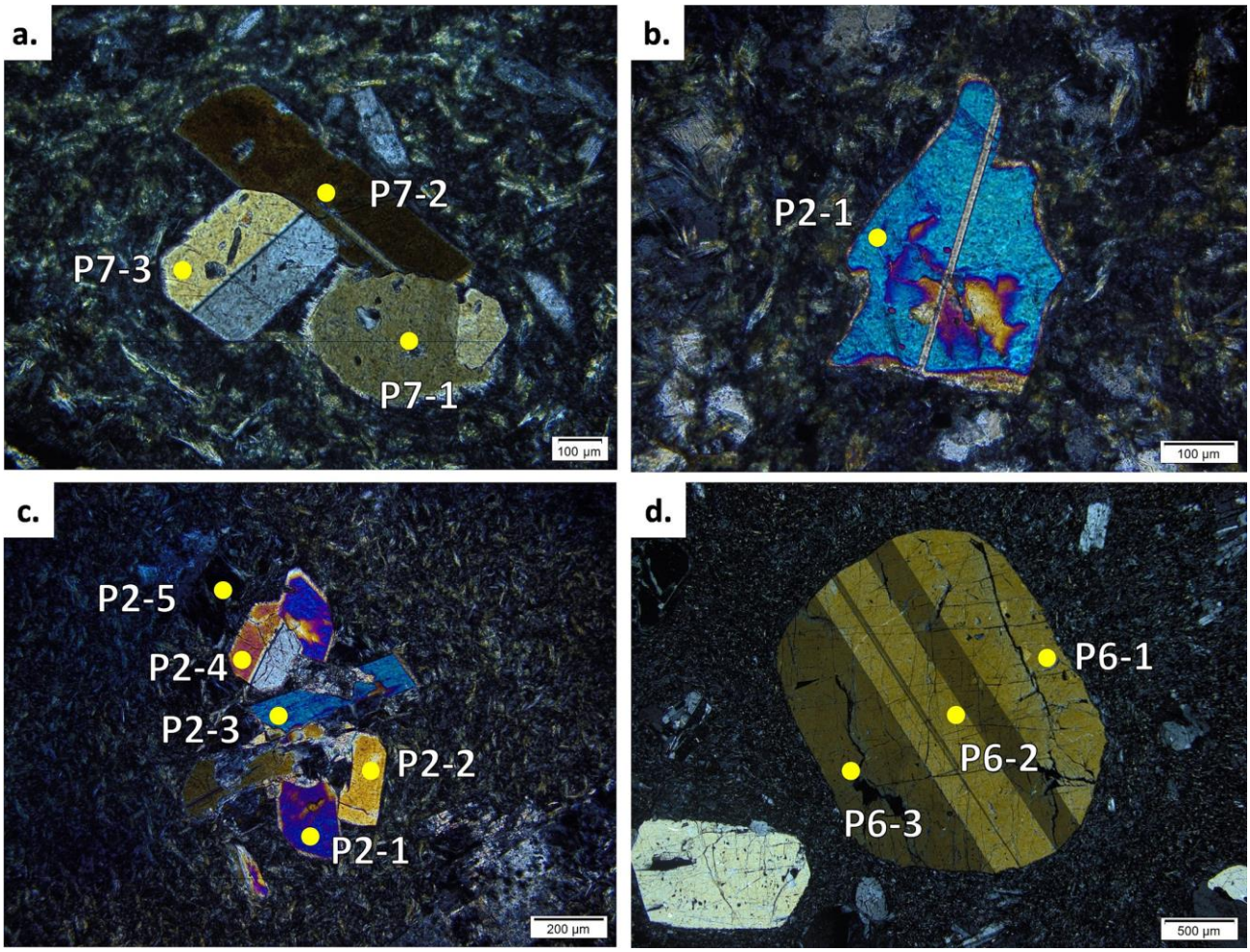

Figure 6. Representative cross-polar images of clinopyroxene phenocrysts from the Caicedo Tuffs and Barroso Formation. **a.** Sample TCR-1232A (Caicedo Tuffs: analyses ID: P7–1, P7–2, P7–3; 20×); **b.** Sample TCR-1232B (Caicedo Tuffs: analyses ID: P2–1; 20×); **c.** Sample TCR-1232C (Caicedo Tuffs: analyses ID: P2–1, P2–2, P2–3, P2–4, P2–5; 10×); **d.** Sample LM-199R (Barroso Formation analyses: P6–1, P6–2, P6–3; 4×).

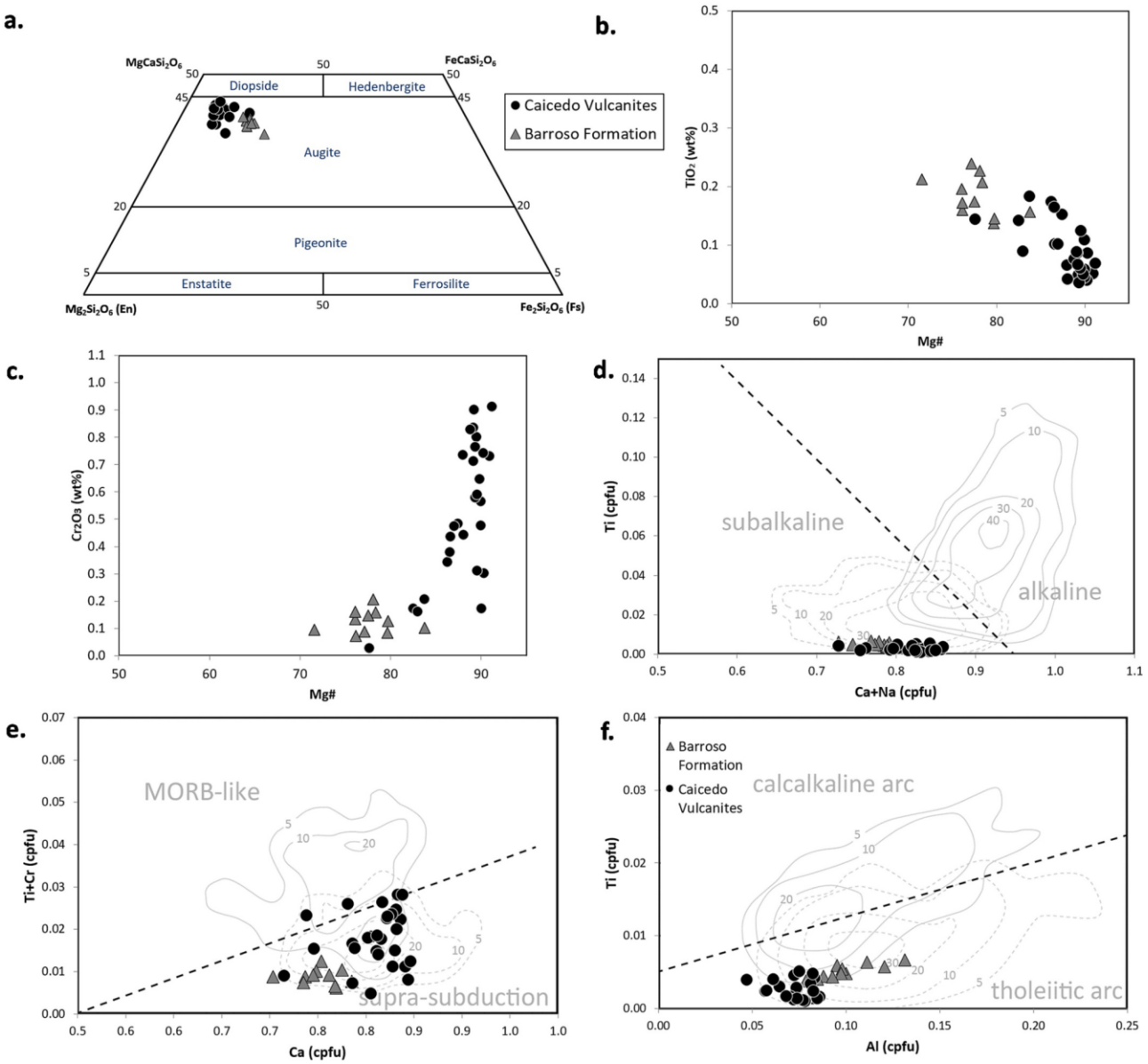

Figure 7. Composition of clinopyroxenes from the Caicedo Tuffs and the Barroso Formation. **a.** Ca-Mg-Fe classification diagram for pyroxene after Morimoto et al. (1988); **b.** Mg# vs.TiO_2; **c.** Mg# vs.Cr_2O_3; **d.** Ca + Na vs. Ti; **e.** Ca vs. Ti + Cr; **f.** Al vs. Ti. Discrimination diagrams (e, f and g) after Leterrier et al. (1982). cpfu: cations per formula unit.

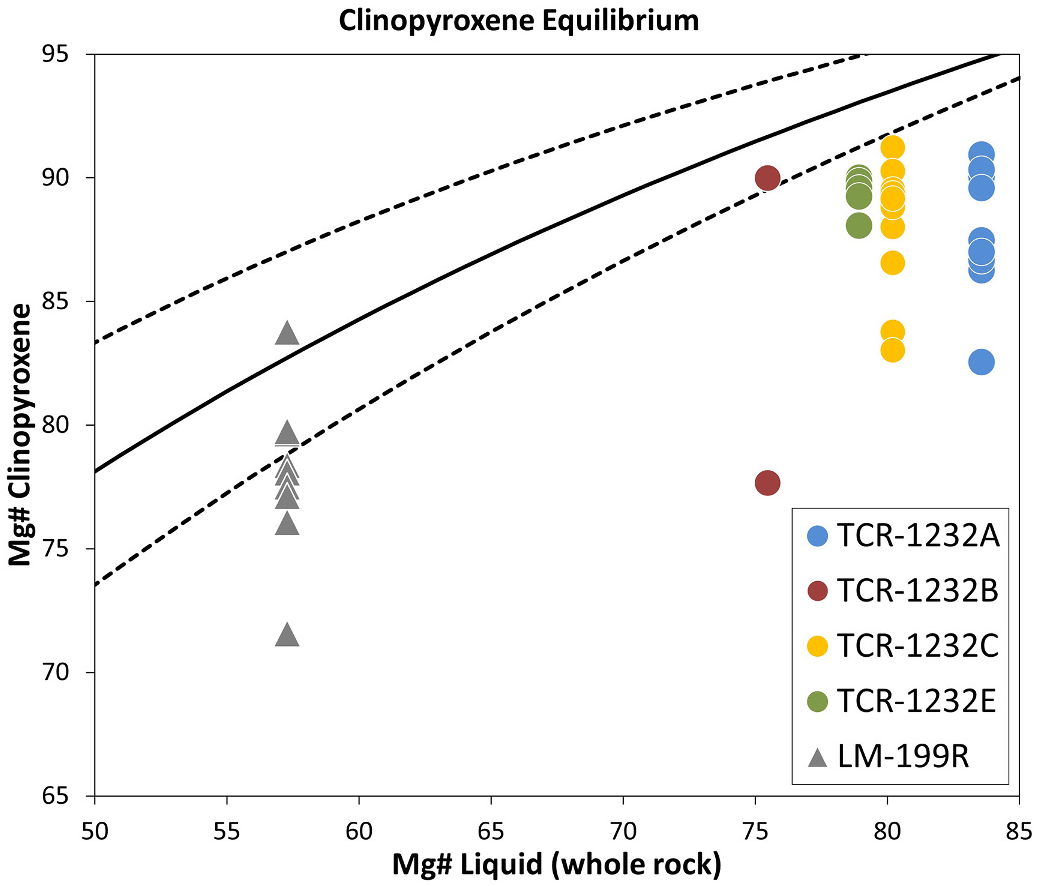

Figure 8. Rhodes diagram with calculated equilibrium curve between clinopyroxenes and their theoretical host melt (estimated from whole rock compositions). Caicedo Tuffs: TCR-1232A, TCR-1232B, TCR-1232C and TCR-1232E; Barroso Formation: LM-199R. KD $(Fe\text{-}Mg)_{cpx\text{-}liq}$ of 0.28 ± 0.08 after Putirka (2008).

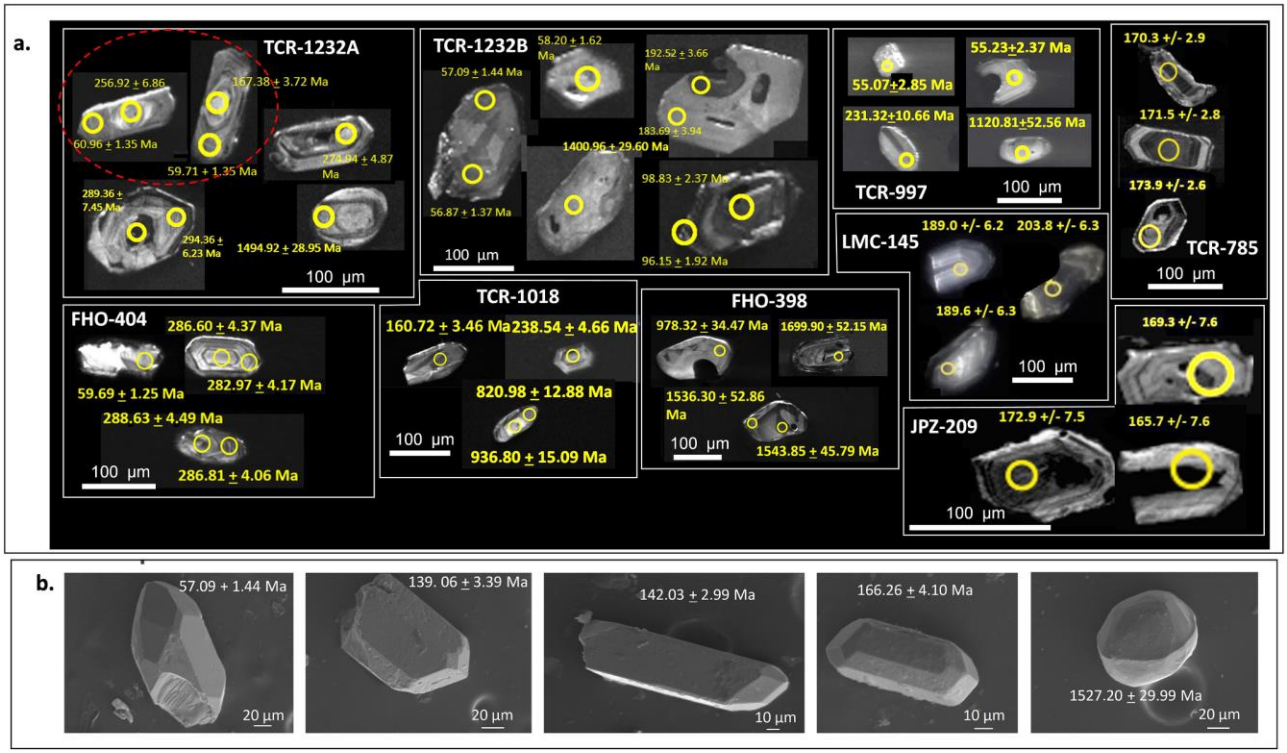

Figure 9. Representative zircons used in the LA-ICP-MS dating process. **a.** SEM-CL Images showing the position of the ablation points and the date obtained for each point (the red dashed ellipse highlights zircons with Paleogene ages in the rim and Jurassic dates in the core; **b.** SEM-BS images of some zircons that were dated showing the more prevalent pyramidal nature of the Paleogene grains vs the more prismatic and often more elongate Jurassic crystals.

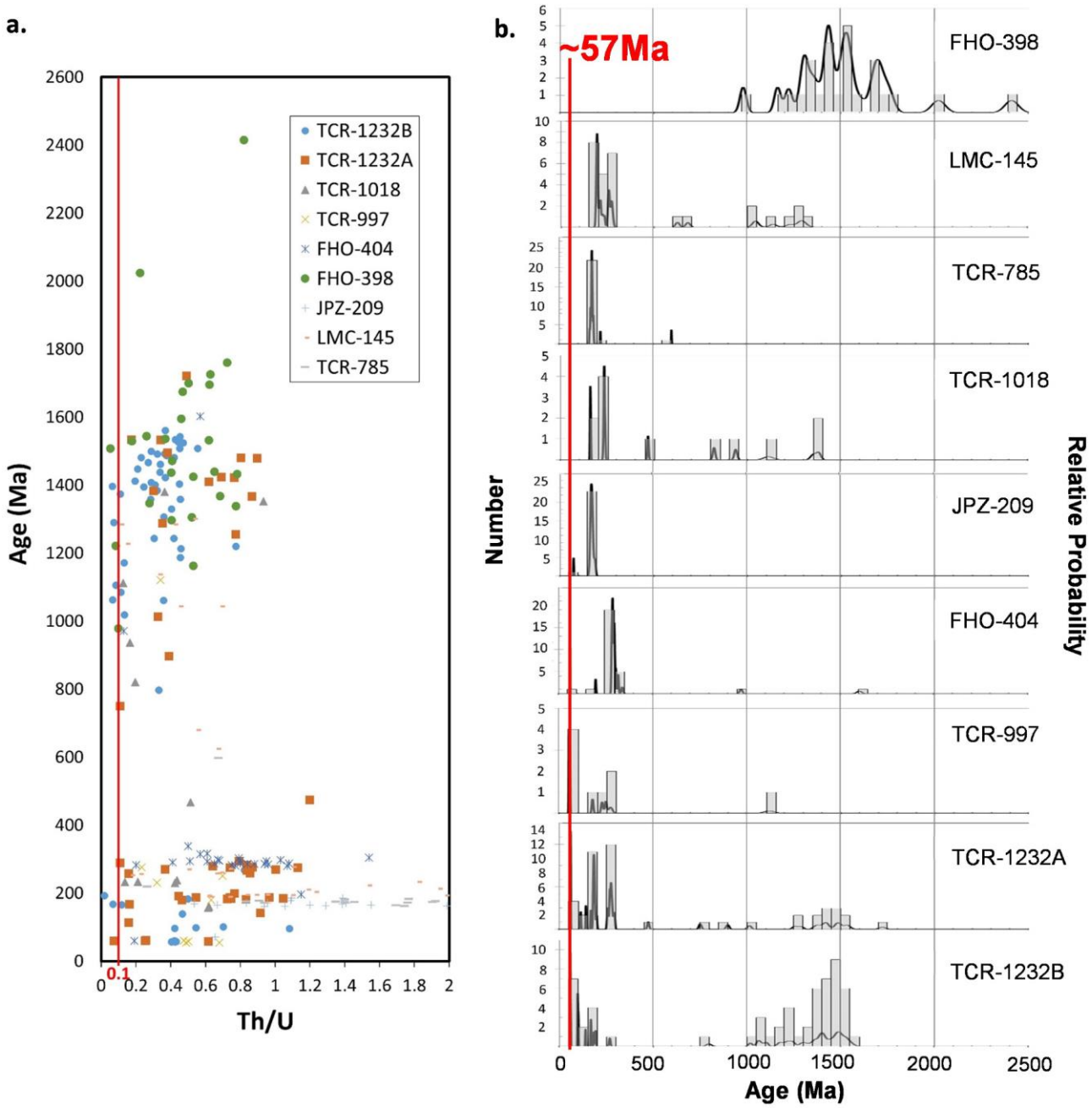

Figure 10. Comparison of data acquired for the zircons analyzed during the LA-ICP-MS dating of the Caicedo Tuffs. **a.** Th/U vs Age (Ma) plot in which the red line indicates the division between igneous and metamorphic events (0.1) according to Rubatto (2002); **b.** Probability density plots of U-Pb ages (the red line indicates the ~57 Ma data found in four of the samples).

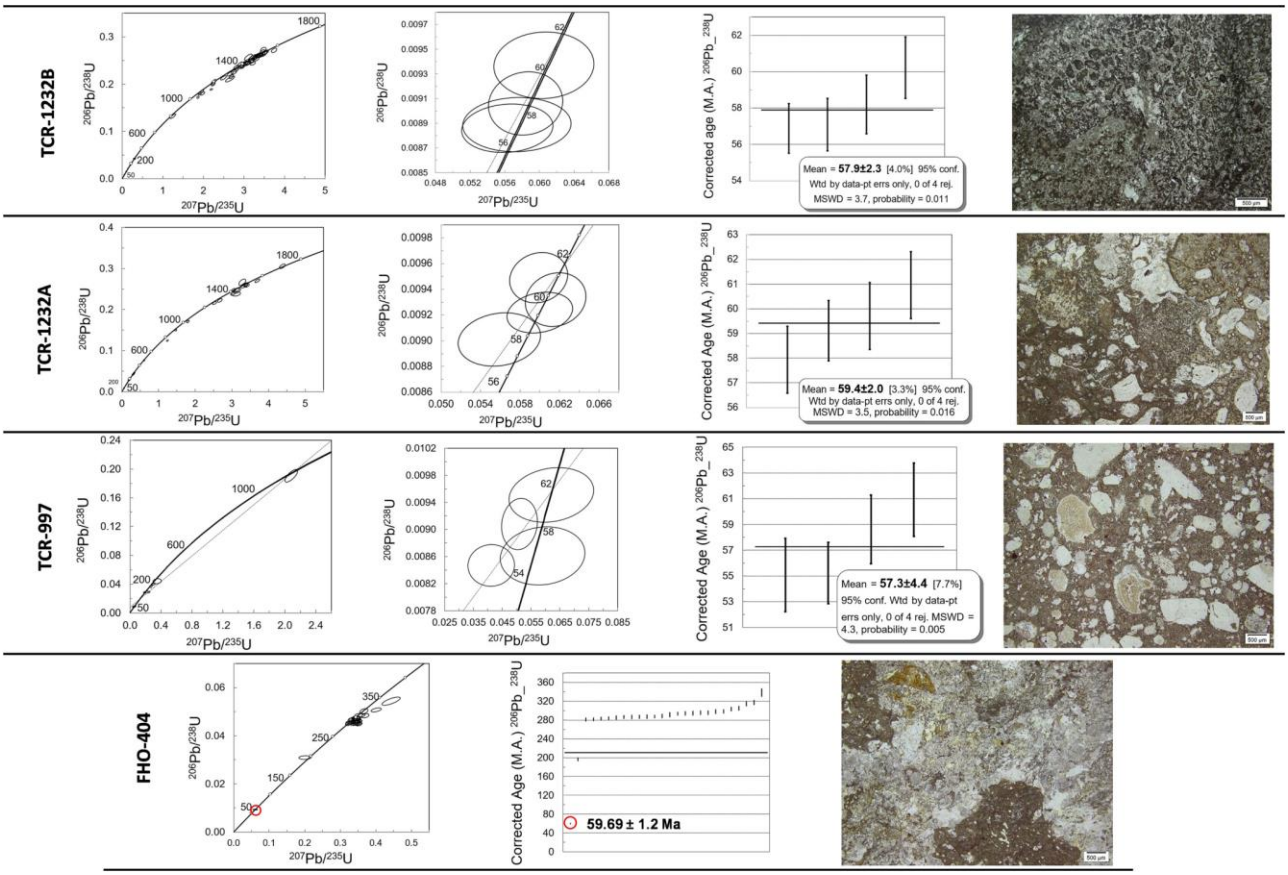

Figure 11. Samples of the Caicedo Tuffs with Paleogene U-Pb in zircon ages. Data point errors are calculated at 2σ for the weighted average and Concordia diagrams. Thin section images are presented to show the textural features of the Paleogene samples. See ST2 for complete isotopic database.

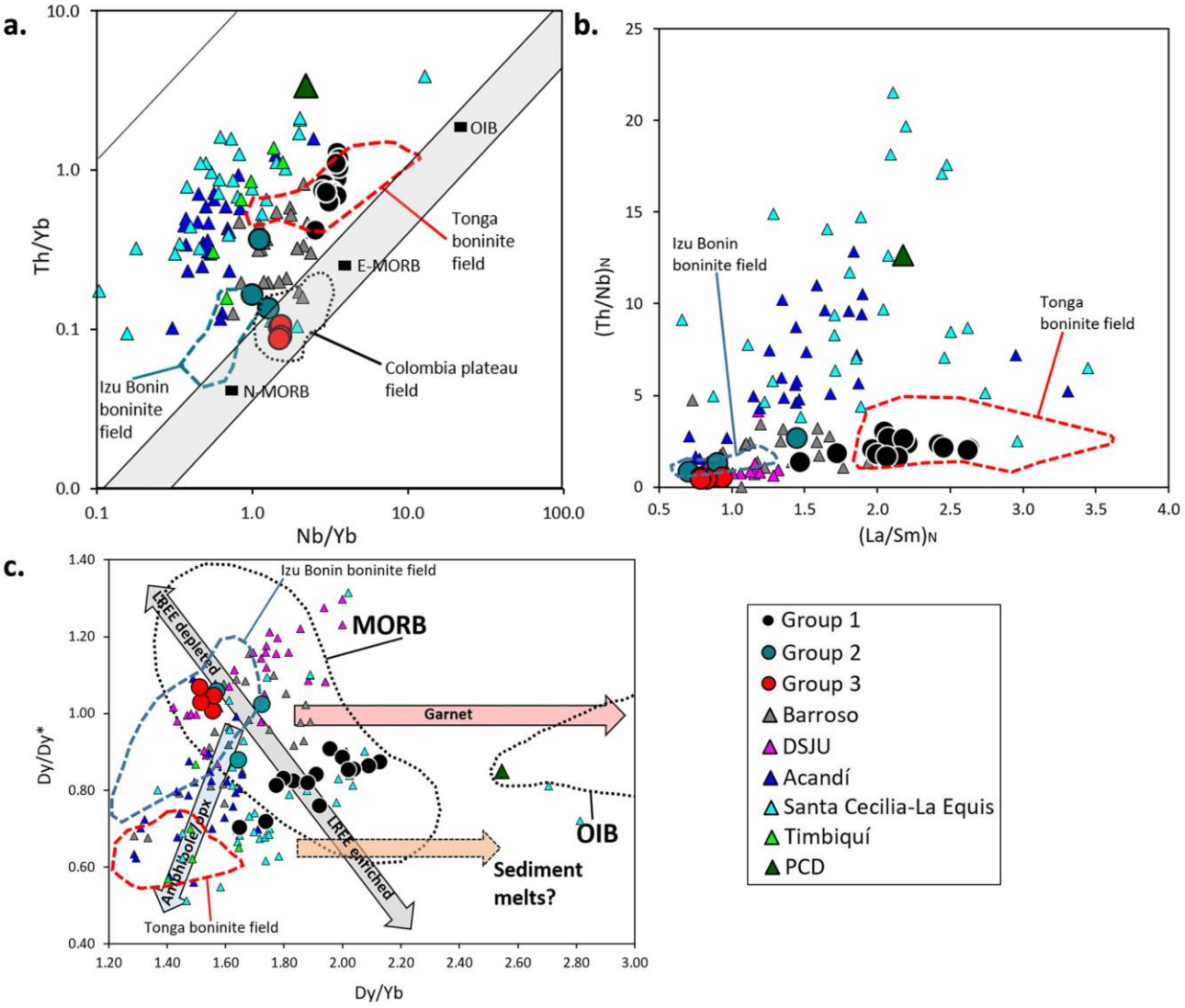

Figure 12. Tectonic discrimination diagrams based on trace elements for Geochemical Groups 1, 2, 3 and the Reference Values. **a.** Nb/Yb vs. Th/Yb diagram (Pearce, 2008); **b.** $(La/Sm)_N$ vs. $(Th/Nb)_N$ diagram; **c.** Dy/Yb vs. Dy/Dy* diagram (Davidson et al., 2013). Reference values for the Barroso Formation and San Jose de Urama Diabases from Rodríguez and Arango (2013); reference values for Acandí, Timbiquí and Santa Cecilia La Equis from Barbosa-Espitia et al. (2019); reference values for the Post Collisional Dyke (PCD) from Zapata-Villada (2018). Values for the Izu-Bonin Boninites field are from Shervais et al. (2021). Values for the Tonga Boninites field are from Falloon et al. (2007, 2008).

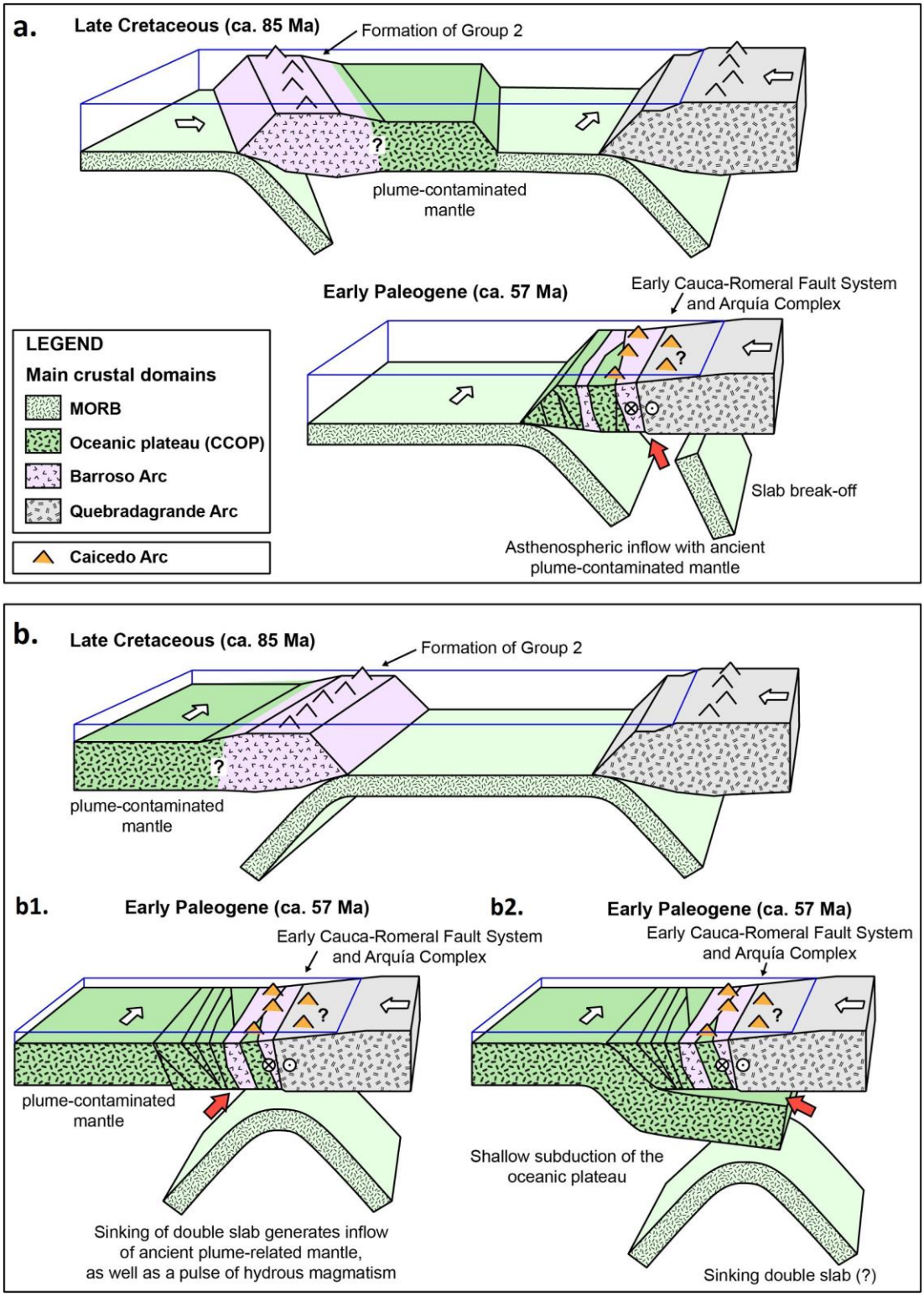

Figure 13. Models of the tectonic evolution of northwestern South America, looking to the north-northeast. Distinct scenarios are proposed to explain the formation of the Caicedo Tuffs in the Paleocene: **a.** East-vergent double subduction with the Late Cretaceous Barroso Arc located above an east dipping slab along the southwestern side of the Caribbean-Colombian Oceanic Plateau (CCOP); **b.** Doubly vergent subduction with the Late Cretaceous Barroso Arc located above a west dipping slab along the southwestern side of the CCOP. In both models the Barroso Arc could locally include an oceanic plateau basement. The Late Cretaceous Quebradagrande arc represents the edge of a marginal basin found further east (not shown in the diagrams). The Caicedo Arc corresponds to Paleocene (Thanetian) magmatism in the study area and nearby Arquía Complex. See Section 5.3 for explanations.